Computational molecular spectroscopy

Published Version:
Computational molecular spectroscopy / Barone, Vincenzo; Alessandrini, Silvia; Biczysko, Malgorzata; Cheeseman, James R.; Clary, David C.; McCoy, Anne B.; DiRisio, Ryan J.; Neese, Frank; Melosso, Mattia; Puzzarini, Cristina. - In: NATURE REVIEWS METHODS PRIMERS. - ISSN 2662-8449. - ELETTRONICO. - 1:1(2021), pp. 38.1-38.27. [10.1038/s43586-021-00034-1]

Availability:
This version is available at: https://hdl.handle.net/11585/867763 since: 2022-02-28

Published:
DOI: http://doi.org/10.1038/s43586-021-00034-1

Computational Molecular Spectroscopy

Vincenzo Barone[1], Silvia Alessandrini[1]
Malgorzata Biczysko[2]
James R. Cheeseman[3]
David C. Clary[4]
Anne B. McCoy[5], Ryan DiRisio[5]
Frank Neese[6]
Mattia Melosso[7], Cristina Puzzarini[7,*]

[1] Scuola Normale Superiore, Piazza dei Cavalieri 7, Pisa, 56126, Italy
[2] International Centre for Quantum and Molecular Structures, Physics Department, Shanghai University, 99 Shangda Road, Shanghai, 200444 China
[3] Gaussian Inc., 340 Quinnipiac St., Bldg. 40, Wallingford, Connecticut 06492-4050, United States
[4] Physical and Theoretical Chemical Laboratory, University of Oxford, Oxford OX1 3QZ, United Kingdom
[5] Department of Chemistry, University of Washington, Seattle, Washington 98195, United States
[6] Max-Planck-Institut für Kohlenforschung, Kaiser Wilhelm-Platz-1, Mülheim an der Ruhr, Germany
[7] Department of Chemistry "Giacomo Ciamician", University of Bologna, Via F. Selmi 2, 40126 Bologna, Italy

*Corresponding author: cristina.puzzarini@unibo.it

Abstract

Molecular spectroscopy techniques are unique tools to probe molecular systems non-invasively and investigate their structure, properties, and dynamics in different environments and physicochemical conditions. Different spectroscopic techniques and their combination can lead to a more comprehensive picture of investigated systems. However, the increasing sophistication of these experimental techniques makes it more and more complex and difficult to interpret the results without the help of computational chemistry. As a consequence, computational molecular spectroscopy has progressively changed from a highly specialized field to a general tool also employed by experimentally-oriented researchers. Computational spectroscopy, born as a branch of quantum chemistry for providing predictions of spectroscopic properties and features, evolved as an independent field. In this Primer, we focus on the characterization of medium-sized molecular systems by means of different spectroscopic techniques. We first provide essential information about the characteristics, accuracy and limitations of the available computational approaches, and select examples with the aim of illustrating general trends, that is outcomes of general validity that can be used for modeling spectroscopic phenomena. We emphasize the need for estimating error bars and limitations, coupling accuracy with interpretability, and discuss the results in terms of widely recognized chemical concepts.

[H1] 1. Introduction

Spectroscopy is the experimental way to study the electronic structure of a system, which is intimately connected to its molecular structure, chemical linkages, and reactivity. Molecular spectroscopy can probe any system in a non-invasive way, thus allowing the investigation of structure and properties in different environments and/or physicochemical conditions. The molecules addressed in this Primer fall into the category of medium-sized systems, which range in dimension from a dozen atoms (such as the smallest amino acid, glycine) to several tens of atoms (e.g. chlorophyll). Almost all possible environments will be considered: from gas phase to solution, to crystals.

Among the various spectroscopic techniques,[1-5] rotational spectroscopy is the most accurate and reliable source for structural information and dynamics of gas-phase molecules.[6-12] Similarly, vibrational spectroscopy permits the characterization of molecules in terms of conformation, chemical linkage, and mutual interactions among atoms and atomic charges modulated by the temperature and environmental effects. Indeed, while rotational spectroscopy is limited to the gas phase, vibrational spectroscopic techniques can also investigate condensed phases. For these reasons, vibrational spectroscopies (infrared, Raman, as well as their chiral counterparts) are commonly employed for characterizing the structure and dynamical behavior of molecular systems. Electronic spectroscopic techniques, in gas or condensed phases, deal with transitions between different electronic states, thus giving access to the characterization of the molecular system in excited electronic states.

Modern high-resolution experimental spectroscopy may involve the acquisition of spectra resolving hundreds, if not thousands of peaks, which is the case, for example, of rotational **[G]** and ro-vibrational **[G]** spectra of polyatomic, asymmetric molecules as well as electron spin resonance (ESR **[G]**) spectra of metalorganic complexes. This spectral overcrowding means the interpretation of high-resolution spectra without the help of quantum chemistry (QC) is a daunting if not impossible task. Indeed, computational spectroscopy, born as a branch of quantum chemistry for providing predictions of spectroscopic properties and features, evolved as an independent field. Currently, theoretical studies in the field of molecular spectroscopy play three roles: interpretation, complementarity, and prediction and support of experimental results. Computational spectroscopy exploits theoretical models, provides tools and computer codes, and validates procedures for the prediction, analysis, interpretation, and understanding of spectroscopic features, properties and/or phenomena. There are several aspects and reasons that contribute to make computational spectroscopy an unavoidable tool in the field of molecular spectroscopy. While there is no room for addressing them in all detail[13-18], in the following we emphasize the topics we consider of primary importance.

In terms of spectral interpretation, spectroscopic experiments often need a broad computational investigation. For example, in order to analyze a recorded rotational or vibrational spectrum of flexible molecular systems, a computational conformational analysis as well as subsequent spectral predictions and simulations are necessary to understand which conformers **[G]** contribute and how. QC also helps identify which aspects of a given structure are responsible for a specific spectroscopic property. Computational studies can establish structure/property relationships as they allow the on or off switching of specific effects and the analysis of the impact of these changes on the simulated spectrum. To give an example, in organometallic complexes, there is a strong relationship between metal-ligand bond distances and Mössbauer isomer shifts **[G]**. Combining broad computational studies with a focus on structure-property relationships can, for example, identify short-lived and unstable species (in either ground or excited states).

In terms of complementarity, one of the goals of experimental spectroscopy is to understand the structure and bonding in molecule, although what is actually measured are the frequencies of light that are absorbed. Computational spectroscopy can act as a bridge between experiments and underlying physical properties, as it provides the theoretical expressions linking observable measurements and molecular properties. Computational and experimental spectroscopy can also be used to benchmark each other.[19] Experimental spectroscopy is extremely sensitive to the electronic structure of a given system, and it is one of the best ways to verify the reliability and accuracy of theoretical predictions and validate QC calculation results. In parallel, experimentally accessible spectroscopic properties may be much more sensitive to molecular structure than total energies, which are often not experimentally measurable.

In terms of prediction and support, the combination of theory and experiment provides experimentally calibrated or experimentally guided insights into electronic structure and, hence, can serve as a guide to the reactivity of systems. The prediction and interpretation of structural properties and dynamic behavior of molecules is at the heart of a deeper understanding of their stability and chemical reactivity. Furthermore, understanding electronic structure and how is reflected in the spectroscopic properties can give insights into entire classes of compounds, rather than only for individual molecules. Computational spectroscopy can also act as the link between different experimental techniques that traditionally were analyzed separately, such as, for example, infrared (IR), Raman, Resonance Raman, ultraviolet–visible absorption or fluorescence (as well as their chiral counterparts), and electron magnetic resonance. QC computations yield direct information on many properties of molecular systems, which can link the molecular properties measured using different experimental techniques. Finally, while peak positions and intensities provide information on the structure of the system, the spectral line-shape is related to dynamical (e.g. fluctuation) aspects. As a consequence, vis-à-vis comparison between simulated and experimental spectra also gives access to these features.

Figure 1 provides a schematic representation of the types of transitions involved in the spectroscopies addressed in this Primer: rotational, vibrational and vibronic spectroscopy. These techniques investigate the transitions between the corresponding energy levels. Together with them, their chiral counterparts, the alternative approach for rotational and vibrational spectroscopies denoted Diffusion Monte Carlo (DMC), and magnetic resonance spectroscopies will be also considered. Figure 1 also allows us to point out the physical aspects underlying each spectroscopic technique. For instance, rotational spectroscopy is related to the rotational motion of the molecular system under consideration, and it can thus be carried out experimentally only in the gas phase. Vibrational spectroscopy describes instead vibrational motion of the atoms within the molecule, and it can be therefore exploited also in condensed phases. The approach mainly followed in this Primer for obtaining the energy levels (DMC being the major exception) is based on effective Hamiltonians and the resolution of the corresponding Schrödinger equation.

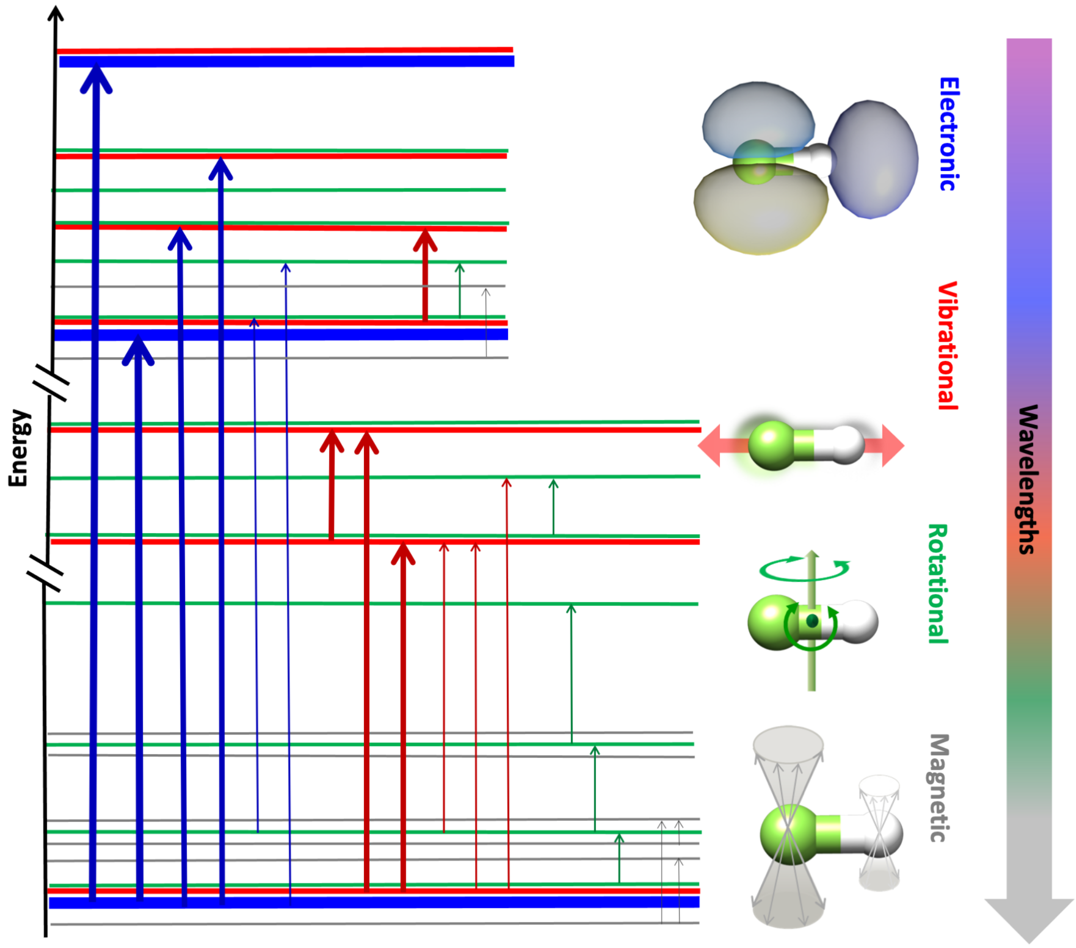

Figure 1. Schematic representation of the energy levels, obtained from the resolution of the opportune Schrödinger equation, and the types of possible transitions. Blue arrows denote the transitions involving a change in the electronic state (from left to right: from thicker to thinner, electronic, vibronic and rovibronic transitions). Red arrows denote the transitions involving different vibrational states (from left to right: vibrational and ro-vibrational transitions). Green arrows denote the transitions only involving rotational energy levels. Dark grey arrows denote the transitions between energy levels obtained from magnetic field splitting.

This Primer is organized as follows. The next section, titled Experimentation, provides the theoretical foundations and computational requirements of the spectroscopic techniques mentioned above. In the subsequent section, some specific results for these spectroscopic techniques are presented, like e.g. the derivation of structural information and the determination of the absolute configuration (AC) **[G]** of chiral molecules. The fourth section, devoted to applications, reports a selection of significant examples such as Astrochemical studies and the characterization of biomolecules and transition metal complexes. In the next two sections the issues of reproducibility and data deposition, and limitations and optimizations will be addressed, respectively. Finally, outlook and perspectives will be provided.

[H1] 2. Experimentation

In the framework of a Primer dedicated to computational spectroscopy, we translate the instrumentation, experimental design, and equipment to the language of the computational world and discuss the theoretical foundations, computational requirements, and codes. In this section, we start with the theory underlying the spectroscopic phenomena associated with molecular systems, attempting to keep the treatment of mathematical expressions as simple as possible. We then move to the computational requirements needed to reach the desired accuracy. We conclude the section with a schematic presentation of some representative computer codes that are currently employed in the field of computational spectroscopy.

[H2] 2.1. Theoretical foundations

The goal of computational spectroscopy is to couple accurate theoretical results with the interpretation of the experimental outcomes by using well-defined models. Theoretical analysis of spectroscopic phenomena is related to the transitions between the energy levels **[G]** (E_{mol}) of a given molecule (see Figure 1), which can be obtained from the solution of the corresponding Schrödinger equation:

$$\widehat{H}_{mol}(\boldsymbol{r},\boldsymbol{R})|\Psi(\boldsymbol{r},\boldsymbol{R})\rangle = E_{mol}|\Psi(\boldsymbol{r},\boldsymbol{R})\rangle \qquad \text{(Equation 1)}$$

where $\widehat{H}_{mol}(\boldsymbol{r},\boldsymbol{R})$ is the molecular Hamiltonian **[G]** (that is the Hamiltonian associated to the molecular system under consideration), with $\boldsymbol{R}$ and $\boldsymbol{r}$ being the position arrays **[G]** of the nuclei and electrons, respectively; $|\Psi(\boldsymbol{r},\boldsymbol{R})\rangle$ is the wave function **[G]** denoting the state of the molecule. As Equation 1 is unsolvable for the majority of the molecular systems, approximations must be introduced in order to obtain energy levels. The Born-Oppenheimer (BO) **[G]** approximation[20] permits the separation of nuclei and electrons motions, thus leading to electronic and nuclear Schrödinger equations. Once nuclear and electronic motions are separated, a further approximation is required to simplify the nuclear Schrödinger equation. This is provided by the Eckart-Sayvetz conditions,[21,22] which factors out the translational motion and minimizes the couplings between vibrations and rotations. One of the major consequences of the BO approximation is the definition of the concept of potential energy surface (PES) **[G]**, which is a function of the nuclear coordinates and provides the relationship between the electronic energy of a molecule (from the resolution of the electronic Schrödinger equation) and its geometry. Stable molecular structures (equilibrium structures) are minima on the PES. A mathematical description of the PES enters the Hamiltonian of the nuclear Schrödinger equation and, to simplify the treatment, it is often expressed in terms of force constants, which are the derivatives of the electronic energies with respect to nuclear coordinates evaluated at the minimum.

Here, we focus on the nuclear Schrödinger equation and, in the following, its resolution by means of perturbation theory techniques is presented. The advantage of perturbation theory is that it is generally accurate, and it is a powerful interpretative tool allowing a direct connection with the parameters that are used by experimentalists to fit their spectra. The most common approach for considering nuclear quantum effects and obtaining the energies and wave functions needed to study spectroscopic properties involves solving the time-independent Schrödinger equation:

$$\widehat{H}_{vr}(\boldsymbol{R})|\Psi_{vr}(\boldsymbol{R})\rangle = E_{vr}|\Psi_{vr}(\boldsymbol{R})\rangle \qquad \text{(Equation 2)}$$

with the Watson Hamiltonian[23] $\hat{H}_{vr}$ being the most widely used Hamiltonian for the description of the vibro-rotational motion of semi-rigid molecular systems. The Watson Hamiltonian is expressed in terms of the dimensionless normal coordinates **[G]** (q) and their conjugate momenta ($\hat{p}$) referred to the equilibrium geometry of the system within a reference frame (principal inertia system) centered in the center of mass and oriented in order to diagonalize the equilibrium inertia tensor **[G]** (Eckart-Seyvetz conditions):

$$\hat{H}_{vr} = \frac{1}{2}\sum_{\alpha,\beta}(\hat{J}_\alpha - \hat{\pi}_\alpha)\mu_{\alpha\beta}(\hat{J}_\beta - \hat{\pi}_\beta) + \frac{1}{2}\sum_r \omega_r \hat{p}_r^2 + V(q) - \frac{1}{2}\sum_\alpha \mu_{\alpha\alpha} \qquad \text{(Equation 3)}$$

where the q are linear combinations of the displacements of the Cartesian coordinates of the atoms. The harmonic wavenumber associated to the r-th normal coordinate is denoted by ω_r, and $\mu_{\alpha\beta}$ denotes an element of the inverse inertia tensor. $\hat{J}_\alpha$ is the rotational angular-momentum operator about axis α, and $\hat{\pi}_\alpha$ represents the α-th component of vibrational angular momentum. Since the exact form of the inverse molecular inertia tensor μ and the potential energy V are unknown, they are expanded as Taylor series with respect to q. A detailed account can be found in refs. [23,24].

A different procedure is offered by a Hamiltonian-independent approach based on inverting the information contained in the experimental spectroscopic transitions **[G]** in order to derive the corresponding energy levels. After collecting all available (experimentally) measured transitions and selecting the most accurate data (i.e. those affected by the low errors), and compiling them into a database, spectroscopic networks are established in order to interconnect the energy levels. A spectroscopic network is a graph where the nodes are the energy levels and the links are the transitions. Inversion of the transitions through a weighted least-squares-type procedure results in the energy levels and associated uncertainties. The MARVEL (Measured Active Rotational-Vibrational Energy Levels) protocol in the field of ro-vibrational spectroscopy[25,26] provides an illustrative example.

[H3] 2.1.1. Rotational Spectroscopy

To address rotational spectroscopy, the first step is the definition of a suitable Hamiltonian. The starting point is the Watson Hamiltonian, from which the rotational part should be extracted. To accomplish this, a contact transformation **[G]** is applied to the vibro-rotational Hamiltonian in Equation 2, and this leads to a block-diagonal effective Hamiltonian.[27] Each of these blocks is labelled in terms of the powers of q and $\hat{p}$, and powers of $\hat{J}$: the power of the former (vibrational) is referred to as *n* and that of the latter (rotational) to *l*. Thus, the vibro-rotational Hamiltonian is now indicated as $\hat{H}_{nl}$. By retaining the pure rotational and centrifugal-distortion terms (i.e. all Hamiltonian terms with *n* = 0), the rotational Hamiltonian is obtained:

$$\tilde{H}_{rot} = H_{02} + \tilde{H}_{04} + \tilde{H}_{06} \qquad \text{(Equation 4)}$$

where $\tilde{H}_{04}$ and $\tilde{H}_{06}$ are the quartic and sextic centrifugal-distortion terms, and H_{02} is the rigid-rotor Hamiltonian:

$$H_{02} = \sum_i B_i^{eq} \hat{J}_i^2 \qquad \text{(Equation 5)}$$

where $\hat{J}_i$ is the projection of the rotational angular momentum operator along the *i*-th inertial axis, and the B_i^{eq} terms represent the equilibrium rotational constants, which are inversely proportional to the corresponding components of the inertia tensor (diagonal in the principal inertia system), which in turn only depends on the equilibrium structure and the isotopic masses of the molecule under consideration.[28] From a computational point of view, equilibrium rotational constants are derived from geometry optimization, the computational procedure that leads to the identification of the equilibrium structure. The accuracy of the equilibrium rotational constants therefore depends on the accuracy of this procedure.

To provide a description of the rotational motion that adheres to the real world, it is mandatory to go beyond the rigid-rotor approximation and include centrifugal distortion ($\widetilde{H}_{04}$, $\widetilde{H}_{06}$, and even higher-order terms)[27,28] in the treatment. In the expression of the centrifugal-distortion terms, the opportune power of the rotational angular momentum operator (which is expressed by the subscript of $\widetilde{H}$) multiplies the centrifugal distortion constants. For the computational determination of the latter, different approximations of the PES entering the Hamiltonian are required: the harmonic **[G]** part for the quartics ($\widetilde{H}_{04}$) and an anharmonic description **[G]** for the sextics ($\widetilde{H}_{06}$). The tilde-sign denotes the result from a Hamiltonian reduction (interested readers are referred to[27,29]). It has to be noted that the Hamiltonian of Eq. 4 applies to the semirigid-rotor approximation case (where the term "semirigid" implies the treatment of centrifugal distortion) and do not take the effect of molecular vibrations into account. For a more accurate and realistic treatment, the terms describing the vibration-rotation interaction need to be incorporated. These lead to the description of the dependence of the rotational and centrifugal constants on the vibrational quantum numbers.

The interactions of the molecular electric and/or magnetic fields with the nuclear or electron (for open-shell species) moments introduce additional terms in the rotational Hamiltonian,[28] and are responsible for the hyperfine structure in rotational spectra (these aspects are detailed later in the text). It should be noted that some of these hyperfine interactions are at the basis of magnetic spectroscopies such as nuclear magnetic resonance (NMR **[G]**)[30] and ESR[30,31] for interaction with nuclear and electron moments, respectively. Although a detailed analysis of those spectroscopies is outside the scope of the present primer, they play a central role in the study of biological molecules and transition metal complexes in condensed phases.[32,33]

[H3] 2.1.2. Vibrational and Vibronic Spectroscopy

The terms of the vibro-rotational Hamiltonian of concern to vibrational spectroscopy are

$$\widetilde{H}_{vib} = H_{20} + \widetilde{H}_{30} + \widetilde{H}_{40} + D \qquad \text{(Equation 6)}$$

where the last term *D* incorporates high-order pure vibrational terms as well as those representing the interaction with the rotational motion (the so-called Coriolis couplings appearing among the latter terms).[23,34] The rigid-rotor harmonic-oscillator model **[G]** corresponds to the first term (H_{20}), and allows to compute wavenumbers (ω) and intensities of the fundamental bands **[G]** (one-quanta transitions from the vibrational ground state) based on second (quadratic) derivatives of energy (quadratic force constants) and first derivatives of properties (e.g. dipole moment for IR spectra or scalar product of electric and magnetic moment for vibrational circular dichroism, VCD[35] **[G]**).

While a harmonic description of the PES entering the vibro-rotational Hamiltonian allows for a simplified description of the vibrational motion, a more realistic picture of the PES requires including anharmonic corrections. However, this complicates the resolution of the corresponding Schrödinger equation, thereby often resorting to perturbation theory. Vibrational perturbation theory to the second order [G] (VPT2)[36,37] offers a very effective solution since the energy levels for all vibrational states can be computed from well-defined combinations of Coriolis couplings together with third and semi-diagonal fourth energy derivatives with respect to normal modes [G] (χ_{ii} and χ_{ij}), leading to the anharmonic wavenumbers for fundamentals, overtones [G], and combination bands [G]:[38]

$$\Delta E_i(0-1) = \nu_i = \omega_i + 2\chi_{ii} + \frac{1}{2}\sum_{i\neq j}\chi_{ij} \qquad \text{(Equation 7)}$$

$$\Delta E_i(0-2) = 2\omega_i + 6\chi_{ii} + \sum_{i\neq j}\chi_{ij} = 2\nu_i + 2\chi_{ij} \qquad \text{(Equation 8)}$$

$$\Delta E_{ij}(0-1,0-1) = \omega_i + \omega_j + 2\chi_{ii} + 2\chi_{jj} + 2\chi_{ij} + \frac{1}{2}\sum_{k\neq i,j}\left(\chi_{ik} + \chi_{jk}\right) = \nu_i + \nu_j + \chi_{ij}$$

(Equation 9)

In analogy, anharmonic intensities can be obtained by a double-perturbative approach [G] in which, for both energy and property, the terms beyond the second and first derivatives, respectively, are treated as perturbations, with the unperturbed reference being the harmonic oscillator Hamiltonian. Computationally, this model requires second- and semi-diagonal third derivatives of the suitable property, with appropriate equations being derived up to three-quanta transitions.[35,39-41]

The most common way to derive the anharmonic PES and property surface (PS [G]) required for VPT2 computations is based on numerical differentiation of the analytical second derivatives of the energy and the first derivatives of the properties.[34,42,43] However, energies and/or gradients can be employed in numerical procedures[42] and, for some electronic structure methods, fully analytical[44,45] derivations have also been reported. When taking into account resonance effects and/or decoupled large amplitude motions by reduced-dimensionality variational approaches, this model is a very effective working-horse for spectroscopic studies, in particular when dealing with medium- to large-sized molecules.[34,35,39] The more so as vibro-rotational couplings can also be written in terms of energy and rotational constant derivatives, without any additional electronic energy computation.[46] In this connection, effective analytical first and second derivatives of methods rooted into the density functional theory (DFT [G]) together with general purpose vibrational perturbation implementations and reduced dimensionality models are allowing for reliable yet feasible anharmonic computations of vibrational (IR, Raman) spectra of large systems and also of their chiral counterparts (for example VCD). Noted is that semi-diagonal third-energy derivatives with respect to normal modes are sufficient to evaluate also first-order vibrational modulation effects on other spectroscopic parameters (e.g. optical activity, hyperfine tensors, etc.).

Together with perturbative approaches, alternative methodologies are possible such as, e.g. vibrational self-consistent field (VSCF),[47] vibrational configuration interaction (VCI),[48] or vibrational coupled clusters (VCC).[49] However, despite recent efforts,[50] they remain much more difficult to translate into black-box procedures to be used also by non-specialists.

Moving to vibronic spectroscopy (vibrational transitions between different electronic states, see Figure 1), vibrational signatures of one-photon absorption (OPA [G]) and one-photon emission (OPE [G]) spectra including chiroptical ones (e.g. electronic circular dichroism, ECD [G]) and resonance regimes (Resonance Raman) are defined by the overlaps between vibrational wavefunctions of the initial (*I*) and final (*F*) electronic states ($\langle\Psi_F(\tau)|\Psi_I(\tau)\rangle$).[51] Small amplitude vibrations can be effectively analyzed by harmonic models,[52,53] which take into account the difference between the normal modes description in the initial (q_I) and final (q_F) states by using the Shift vector, $\boldsymbol{K}$, and the Duschinsky rotation matrix,[54] $\boldsymbol{J}$):

$$q_I = \boldsymbol{J} q_F + \boldsymbol{K} \qquad \text{(Equation 10)}$$

Strong, bright electronic transitions can be simulated in terms of equilibrium transition dipole moments, d_{IF} (Franck-Condon approach[55,56]), whereas inclusion of the transition dipole moment first derivatives with respect to normal coordinates becomes mandatory for forbidden or weakly-allowed transitions (Herzberg-Teller term[57]):

$$\left[d_{IF}^{eq}\langle\Psi_F(\tau)|\Psi_I(\tau)\rangle\right]^{FC} + \left[\sum_n \frac{\delta d_{IF}^n}{\delta q}\langle\Psi_F(\tau)|\Psi_I(\tau)\rangle\right]^{HT} \qquad \text{(Equation 11)}$$

with the sum over *n* (in the second term) running over the 3N-6 normal coordinates (3N-5 for linear molecules, N being the number of atoms of the molecule). Finally, for flexible molecular systems internal (in place of cartesian) coordinates must be employed whenever curvilinear effects cannot be neglected (as it is usually the case for low-frequency modes like, e.g., torsions, inversions or ring puckerings),[58,59] and possibly also integrated with one-dimensional variational models for decoupled large amplitude motions[60]. The considerations above are limited to those cases where the BO approximation applies. More advanced treatments, also including non-adiabatic contributions, are needed for more involved situations (e.g. near conical intersections).

A sketch of the main spectroscopic techniques, which can be reliably simulated in this framework is given in Figure 2, while for additional tutorial and review see refs.[34,61,62]

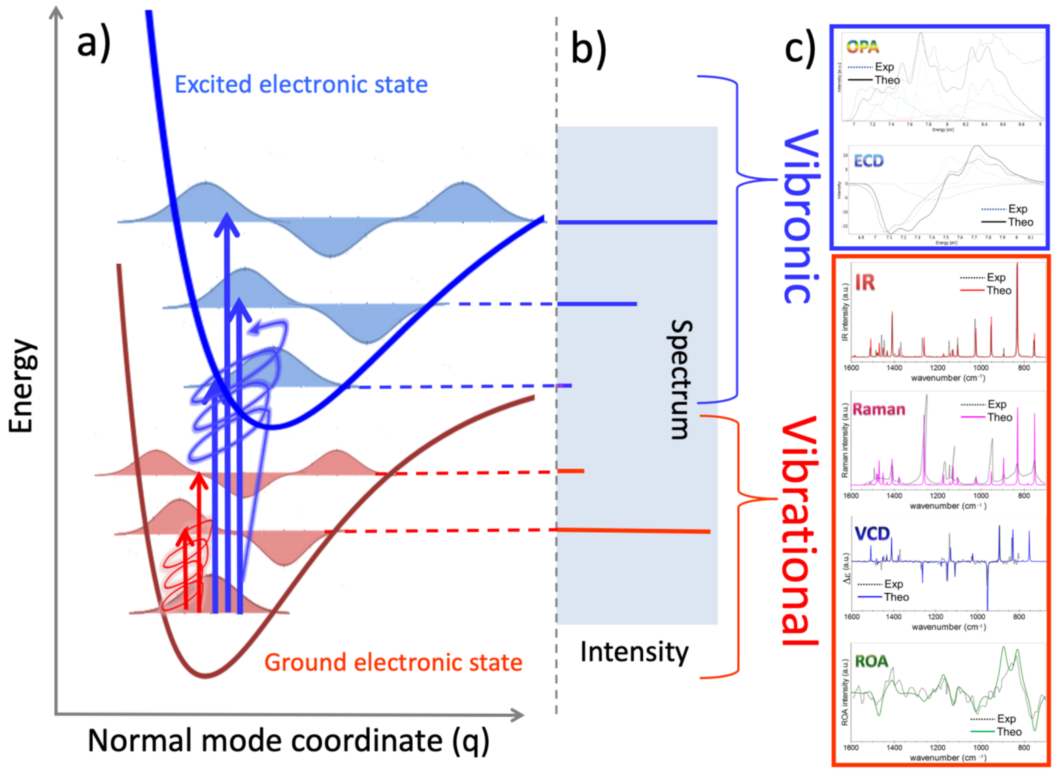

Figure 2. General theoretical framework for vibrational and vibronic spectroscopies, and their chiral counterparts. Panel (a): schematic representation of the ground (red) and excited (blue) electronic state PESs, vibrational energy levels and wavefunctions. The energy scale underestimate gap between the two electronic states. Straight arrows represent transitions from the vibrational ground state: vibrational (red; IR and Raman) and vibronic (involving both states, blue; OPA). Circled arrows stand for the interaction with circularly polarized light corresponding to VCD (red), ROA (red) and ECD (blue) spectroscopies. Panel (b): schematic representation of resulting vibrational and vibronic line positions and corresponding intensities. Panel (c): examples of simulated and experimental spectra from refs [17,35] .

[H3] 2.1.3. Chiral Spectroscopy

The chiral spectroscopic techniques addressed in this Primer are limited to optical rotation (OR), ECD and VCD, as well as Raman optical activity (ROA **[G]**). OR and ECD arise from the differential refraction and absorption, respectively, for left and right circularly polarized light and are associated with electronic transitions. Optical rotatory dispersion (ORD **[G]**) is the wavelength dependence of the OR. VCD and ROA arise from the differential absorption and scattering, respectively, for left and right circularly polarized light and are associated with vibrational transitions. The approximations and models related to the vibrational wavefunctions and their overlaps are the same as described in the previous section (2.1.2).

ORD is determined by the electric dipole – magnetic dipole polarizability, which is computed using linear response methods as implemented in different QC software packages.[63-65] Specifically, QC programs report the specific rotation at each incident frequency in units of degrees dm^{-1} $(g/mL)^{-1}$, which can then be compared directly with the experiment. ECD and VCD are determined by the dipole and rotational strengths of electronic or vibrational transitions, respectively, which are related to the scalar products of the electric dipole and magnetic dipole transition moments. For VCD, these are computed using linear response methods at either the harmonic[1,66,67] or anharmonic[35] level. The experiments measure the differential absorbance for left and right circularly polarized light, which is typically converted to the differential molar extinction coefficient $\Delta\epsilon$ (in units of M^{-1} cm^{-1}), which is related to the absorbance through Beer's Law[68] . Since experimental band-shapes of VCD spectra are most frequently Lorentzian while the experimental band-shapes of ECD spectra tend to be Gaussian, the appropriate line-shape function **[G]** is added to the calculated $\Delta\epsilon$. For more detail and the relevant conversions, the reader is referred to [1,66,69] for VCD and [69,70] for ECD.

ROA is determined by electric, magnetic, and quadrupole polarizability transition moments of vibrational transitions that are computed using linear response methods at either the harmonic[67,71,72] or anharmonic[35] level. In the far-from-resonance theory, where the exciting laser radiation is far from the lowest allowed electronic excited state, ROA intensity differences are determined by three tensor invariants constructed as linear combinations of products of these polarizability tensors.[1,69,73,74] Depending on the choice of polarization modulation and scattering geometry, several forms of ROA are obtained, although the most common is back scattered circular polarization denoted as SCP(180). QC programs report the ROA scattering activities for a particular experimental setup, which are then converted to a differential scattering cross section which includes a factor of $(\nu_{inc} - \nu_i)^4$, where ν_{inc} and ν_i are the wavenumbers for the incident frequency and mode i, respectively[69,75,76] Since experimental band shapes are typically Lorentzian, calculated spectra are plotted using the Lorentzian line-shape function. As absolute ROA intensities are not typically measured, it is common practice to label the intensity differences as $I_R - I_L$, as is done for the experimental spectra.

[H3] 2.1.4. Diffusion Monte Carlo (DMC)

An alternative to conventional time-independent computational approaches to rotational and vibrational spectroscopy is offered by propagation of the time-dependent Schrödinger Equation as

$$|\Psi(\tau)\rangle = \sum_n c_n e_n^{-\tau(E_n - V_{\text{ref}})} |\phi_n\rangle \qquad \text{(Equation 12)}$$

where $|\phi_n\rangle$ is an eigenstate of the Hamiltonian, with energy E_n[77-86] and $\tau = it/\hbar$. When we propagate an arbitrary wave function in imaginary time, at long times the leading contribution to the wave function will be the ground state. Further, if $V_{\text{ref}} = E_0$, the amplitude of the wave function will remain constant. The advantage of DMC approaches over conventional approaches comes in the representation of the wave function. In the simplest implementation of diffusion Monte Carlo, $|\Psi(\tau)\rangle$ is represented by an ensemble of localized functions, $g(\boldsymbol{x} - \boldsymbol{x}_i)$,

$$\langle \boldsymbol{x}|\Psi(\tau)\rangle = \sum_i w_i(\tau) g(\boldsymbol{x} - \boldsymbol{x}_i) \qquad \text{(Equation 13)}$$

At each time step in the simulation, each of the components of each of the $\boldsymbol{x}_i$ is displaced by a random value based on Gauss-random distributions, where the distribution for the jth atom has a width of $\sqrt{\frac{\Delta\tau}{m_j}}$, where m_j represents the corresponding mass. After the atoms are displaced, the potential energy is evaluated, and the weight $w_i(\tau)$ is adjusted according to

$$w_i(\tau + \Delta\tau) = e^{(V(x_i) - V_{\text{ref}})\Delta\tau} w_i(\tau) \qquad \text{(Equation 14)}$$

This relatively simple algorithm provides a Monte Carlo sampling of the ground state wave function for the molecule of interest based on the provided potential surface as well as the ground state energy. By propagating the ensemble forward in time we can obtain the information required to generate the ground state probability amplitude.[84,87] Such information allows us to explore how the molecule samples the potential and evaluate, for example, rotational constants for obtaining rotational spectra. Finally, energies and wave functions for rotation or vibrationally excited states can be obtained using this approach by imposing a nodal structure for these states.[86,88,89] The major advantage of DMC over more conventional approaches is that it allows a way to explore the role of nuclear quantum effects in systems where the ground state wave function is delocalized among multiple local minima on the potential surface. These are situations where approaches, like perturbation theory, become less effective.

[H2] 2.2. Software for computational spectroscopy

Some available QC packages together with their potentialities and main features are provided in Table 1.

Table 1. Selection of common software packages for computational spectroscopy applications: QC methodologies and main spectroscopic features.

Software package	Methodology	Spectroscopic applications
CFOUR http://www.cfour.de/ [academic]	CC theory / MP2 (analytic 2nd derivatives) CC composite schemes	Rotational spectroscopy: all parameters Vibrational spectroscopy: VPT2 NMR/ESR spectroscopies: all parameters
Gaussian https://gaussian.com/ [commercial]	DFT/TD-DFT/MP2 (analytic Hessians) CCSD(T) energies QM/QM'/MM/PCM	Rotational spectroscopy: all parameters Vibr. Spectroscopy: IR, Raman, VCD, ROA Electr. Spectroscopy: UV-Vis, ECD, RR, RROA NMR/ESR spectroscopies: all parameters
Molpro https://www.molpro.net/ [commercial]	CC and explicitly correlated CC Multireference methods DFT/TD-DFT	Rot. Spectroscopy: equilibrium rot. constants Vibrational Spectroscopy: VSCF/VCI
NWCHEM https://nwchemgit.github.io/ [academic]	CC theory energies MP2 analytical gradients DFT/TD-DFT QM/MM COSMO/SMD/VEM	Rot. spectroscopy: equilibrium rot. constants Vibration spectroscopy: VSCF energies Electr. Spectroscopy: UV-Vis NMR: shielding tensors and indirect spin-spin coupling

ORCA https://orcaforum.kofo.mpg.de/app.php/portal [academic]	CC and explicitly correlated CC Local correlation methods Multireference methods DFT/TD-DFT QM/MM, Embedding schemes Implicit solvation	Rot. Spectroscopy: equilibrium rot. constants Vibr. Spectrosc.: IR, Raman, res. Raman, NRVS Electr. Spectroscopy: UV-Vis, ECD, MCD, Fluorescence, Phosphoresence, Band shapes NMR/ESR spectroscopies: all parameters X-ray absorption/emission, RIXS, Mössbauer
QChem http://www.q-chem.com/ [commercial]	CC theory (ground and excited states, spin-flip methods), MP2/ADC schemes (energies and gradients) DFT/TD-DFT QM/MM PCM	Rot. spectroscopy: equilibrium rot. constants Vibrational spectroscopy: IR/Raman, anharmonic energies TOSH, VPT2, VCI Electronic Spectroscopy: UV-Vis, RR
PSI4 http://www.psicode.org [academic]	CC /MP2 CCSD(T) gradients CC/MP2 composite schemes for energies, gradients and Hessians DFT/TD-DFT Solvent via external codes	Spectrosc. constants for diatomics from PES fit Rot. spectroscopy: equilibrium rot. constants Vibrational spectroscopy: harmonic models, Electronic Spectroscopy: UV-Vis, OR

[H2] 2.3. Computational requirements

The computational requirements strongly depend on the type of spectroscopic technique under consideration and the accuracy specifically required.

In the case of rotational and vibrational spectroscopies, the leading properties to be accurately computed are the equilibrium rotational constants (which means equilibrium structure determinations) and the harmonic frequencies (which implies harmonic force-field evaluations), respectively. To obtain accurate results, one has to put effort on the electronic structure calculations, the key point being to reduce as much as possible the errors due to the truncation of both basis set (one-electron error) and wavefunction (N-electron error). To achieve this goal, composite schemes have been set up: these evaluate the contributions important to reach high accuracy at the best possible level and then combine them through the additivity approximation (see, e.g., refs. [90-102]). These usually involve the coupled-cluster (CC) theory **[G]** [103] and in particular the CC single and double excitations and a perturbative treatment of triples (CCSD(T)) **[G]** method[104], which is often denoted as the “gold standard” for accurate calculations. On the other hand, the introduction of explicitly-correlated (F12) treatments[105] allows for partially recovering the one-electron error without extrapolation techniques. The development of local-correlation treatments based on pair natural orbital (PNO **[G]**)[106,107] allows instead for improving the scaling of coupled cluster treatments with the number of electrons.

From a computational point of view, going beyond the rigid-rotor harmonic-oscillator approximation increases the complexity and the cost of electronic structure calculations, thus requiring a reduction of the level of theory for the electronic computations as well as the introduction of approximations for the solution of the nuclear problem. Concerning the former issue, global-hybrid or double-hybrid density functionals[108-110] **[G]** provide an optimal alternative to low-cost ab initio methodologies such as the Møller-Plesset theory to second order (MP2)[111], while VPT2 offers a powerful tool for the latter. The definition of hybrid coupled cluster/density functional theory (CC/DFT) models, employing anharmonic corrections and/or property predictions beyond the electric dipole moment from DFT, have been shown to represent nearly optimal compromises between feasibility and accuracy.[35,112,113]

However, application of DFT approaches to computational spectroscopy studies requires careful benchmarking of all the required properties. Unfortunately, most of the benchmark studies reported so far have been focused on the accuracy of energetic properties, for selected equilibrium structures,[114-117] whose conclusions cannot be directly transferred to assess the accuracy of wider regions of the PES (1) or other properties (2).[62,118-120] Concerning the issue 1, flexible systems (like, e.g., most biomolecules) are governed by flat potential energy surfaces, whose behavior cannot be described in terms of the well-separated energy minima within nearly-harmonic basins, which have been considered in most benchmarks. Focusing on point 2, the interpretation of important spectroscopic techniques requires properties (e.g. magnetic dipole moments for chiroptical techniques), whose computation has -however- not yet been validated in a comprehensive way. Moreover, often second and higher analytical derivatives (of energy and properties) are not implemented for some of DFT models, hampering their application in computational spectroscopy studies. As a matter of fact, only a limited number of functionals and basis sets have been benchmarked for geometric structures,[120-126] anharmonic vibrational frequencies,[62,118,119,126,127] and other spectroscopic properties.[119,126] The situation is less advanced for excited electronic states, but the first benchmark studies going beyond vertical excitation energies have been reported[128,129]. Moreover, the recent implementation of analytical TD-DFT Hessians allows more efficient VPT2 computations for excited electronic states of medium- to large-sized molecules.[130] A more reliable, but much more computational expensive alternative to DFT is offered by highly accurate Equation-of-Motion-CC (EOM-CC **[G]**)[131]. Nevertheless, despite the successful applications of these approaches, multireference (MR) methods[132] cannot be avoided whenever nondynamic (static) correlation **[G]** is important. Indeed, MR methods being based on wave functions described by the linear combination of several electronic configuration are able to well address strong correlation effects. We note in passing that modern linear or low-order scaling local correlation methods (based on MP2 or CCSD(T)) have found increasing use in quantum chemistry and also in theoretical spectroscopy[133-135] However, a more detailed description of these aspects is out of the scope of this Primer.

The most generally applicable methods in transition-element theoretical spectroscopy (see section 4.3) are based on traditional[18] or more recent (e.g. density matrix renormalization group **[G]**, DMRG[136]) multireference wavefunction based theories. These methods can now be routinely applied to larger molecules (100-200 atoms). While they have been used extensively in form of, for example, complete active space perturbation theory to second order (CASPT2 **[G]**)[137,138] or N-electron valence state perturbation theory to second-order (NEVPT2 **[G]**)[139], severe limitations still exist that will provide incentive for method developers for decades to come. A more thorough description of these approaches and their strengths and weaknesses is outside the scope of this Primer.

A non-exhaustive summary of the computational evaluation of spectroscopic parameters is provided in Table 2, where - for each spectroscopic technique considered in this Primer - the (best) accuracy obtainable, the type of computation required as well as the level of theory and the affordable dimension of the system are collected. Noted is that this table is based on analytical derivative techniques, which means that further extensions in terms of properties and levels of theory can be reported.

[bH1] Table 2. QC methodologies for the evaluation of spectroscopic parameters and associated accuracy.

Spectroscopy	Spectroscopic parameters	Accuracy	QC calculations	QC methodology & feasible number of atoms	
				Wave function	DFT
Magnetic	• Chemical Shifts • Spin-Spin Coupling • g-tensor • Zero-Field splitting • Hyperfine coupling • Quadrupole coupling • Magnetizability	Moderate; Variable for different nuclei	Response property calculation for imaginary and triplet perturbations	CCSD(T) < 10 Local CCSD(T) <200 (Local) MP2 < 200 HF < 1000	GGA < 2000 Hybrid < 1000 Double hybrid < 100
Nuclear	• Mössbauer • NRVS	10^{-9} eV <10%	Isomer shift, Quadrupole splittings, low-energy vibrational modes	CCSD <10 DLPNO-CCSD < 100	DFT < 1000
Rotational	• Rotational constants Equilibrium Vibrationally corrected	 <0.1% - 0.5% 0.1% - 2%	 Geometry optimization (minimum of the PES) Anharmonic force field (2nd and 3rd energy deriv.)	 Composite schemes < 30 MP2 < 20 CCSD(T) < 10	 Hybrid > 100 Double-hybrid < 100 Hybrid < 100 Double-hybrid < 20
	• Centrifugal (quartic) distortion constants	<1%	Harmonic force field	Composite schemes < 15	Hybrid <30 Double-hybrid < 20
Vibrational	• Vibrational freq. Harmonic Anharmonic (VSCF/ VCI/ VPT2)	 1-20 cm^{-1} 1-10 cm^{-1}	 Harmonic force field Anharmonic contributions (3rd + 4th energy derivatives)	 Composite schemes < 15 MP2 < 20 CCSD(T) < 10	 Hybrid < 400 Double-hybrid < 50 Hybrid < 50 Double-hybrid < 20
	• IR/Raman intensities Harmonic Anharmonic	 10 km mol^{-1} 5 km mol^{-1}	 dipole mom./polarizability: 1st der. wrt to nucl. coord. dipole mom./ polarizability: 2/3 der. wrt to nucl. Coord	 Composite schemes < 15 MP2 < 20 CCSD(T) < 10	 Hybrid < 100 Double-hybrid < 50 Hybrid < 50 Double hybrid < 20
	• VCD/ROA intensities Harmonic Anharmonic	 10-30%	 Magnetic moments: 1st der. wrt to nucl. coord. Magnetic moments: 2/3 der. wrt to nucl. coord.		 Hybrid < 100 Hybrid < 50
Vibronic	• Electronic energy	0.1 -0.5 eV	Initial - final state energy difference between	MRCI, ADC EOM-CCSD <50 DLPNO-STEOM-CCSD < 150	TD-DFT < 200 TDA < 2000
	• Ground state equilibrium structure, normal modes and frequencies	(see Rotational and Vibrational)			
	• Excited electronic state equilibrium structure	0.02-0.1 Å	Geometry optimization (minimum of the PES)	ADC(2) <50 EOM-CCSD,CC3 <15	TD-DFT < 100 TDA < 200
	• Excited electronic state normal modes and Harmonic frequencies Anharmonic frequencies	30 cm^{-1} 10 cm^{-1}	Harmonic force field (analytical or numerical differentiation of analytical gradient) Anharmonic contributions (3rd + semi-diag. 4th deriv.)	EOM-CCSD < 20 MRCI, EOM-CCSD < 6	TD-DFT < 100 TDA < 200 TD-DF T <20
	• OPA/OPE/ECD • FC/HT	0.2 eV 0.05 eV	Electric and/or magnetic transition moment Transition moment derivatives	EOM-CCSD, CC3 < 15	TD-DFT < 100 TDA < 200 TD-DFT < 100
X-ray	• K-edge absorption • L-edge absorption • K-beta emission • RIXS	1 eV 10% relative intensity	Excitation energies Multipole transition moments	EOM-CCSD < 20 MRCI < 10 NEVPT2 < 200 (RO-)CIS < 1000	TD-DFT < 1000

[H1] 3. Results

In this section a few spectroscopic techniques have been selected to provide examples of how to process, treat and interpret spectroscopic data, specifically for spectroscopies involving rotational and vibrational motions.

[H2] 3.1. Rotational Spectroscopy for structural information

Despite the fact that rotational spectroscopy is the technique of choice for structural determinations, such derivations are seldom straightforward. Indeed, extracting geometrical parameters from the experimental information (rotational constants) is hampered by the number of data (rotational constants) actually available and vibrational effects.[6] The fruitful interplay of high-resolution spectroscopy and QC allows for overcoming such difficulties, thereby exploiting a semiexperimental approach.

The semiexperimental approach leads to equilibrium structures (i.e., by definition, the geometries corresponding to minima on the PES) by least-squares fitting the structural parameters to the semiexperimental equilibrium rotational constants ($B_{i,e}^{SE}$), which are determined by subtracting the computed vibrational corrections ($\Delta B_{i,0}^{calc}$) from the experimental (vibrational) ground-state rotational constants ($B_{i,0}^{exp}$):[6]

$$B_{i,e}^{SE} = B_{i,0}^{exp} - \Delta B_{i,0}^{calc} = B_{i,0}^{exp} + \frac{1}{2}\sum_n \alpha_i^n \qquad \text{(Equation 15)}$$

where *i* denotes the principal inertial axis (a, b or c; so that $B_{i=a} = A$); the α_i^r are the so-called vibration-rotation interaction constants and the sum is taken over all fundamental vibrational modes *n.*[28] As evident from Eq. 15, resorting to equilibrium rotational constants allows to get rid of vibrational effects (via the subtraction of the vibrational corrections). To overcome the limitation of the number of experimental data (for a given isotopologue, there are at most three rotational constants), different isotopic species are considered. In fact, these share the same equilibrium structure because, within the BO approximation, the PES of a given molecule is isotope independent. At the same time, they have different equilibrium rotational constants (because they depend on the equilibrium structure and on the isotopic masses), thus increasing the amount of experimental data. A sufficient number of isotopic species is required to have enough information for a complete structural determination (i.e. to have more data than geometrical parameters). This procedure is graphically described in Figure 3. Vice versa, high-level QC calculations allow accurate predictions of the rotational parameters[140] to be used for planning, guiding, and interpreting experiment.[34] Such an interplay can be enhanced by exploiting graphical tools able to visualize, compare and manipulate spectra as well as to handle their assignment.[141]

While these accomplishments are well established for small to medium-sized, semi-rigid molecules (such as those shown in Figure 3), the situation is more involved for larger (and usually less rigid) molecular systems. In recent years, thanks to the introduction of laser ablation vaporization[142] and broadband[9] techniques, the targets of spectroscopic studies have been shifting towards flexible molecules as well as non-covalent molecular complexes involving more than two molecules, both categories being characterized by a large number of closely spaced energy minima (conformers or isomers), all contributing to the overall spectrum. Therefore, a correct analysis of the latter requires the knowledge of the rotational spectra of all isomers and/or conformers present in the gas-phase mixture. Then, by weighting each contribution according to its population, the overall rotational spectrum is obtained. Therefore, an incomplete account of conformers [G] can easily generate an unsatisfactory modeling; the situation is similar to the case of a wrong equilibrium structure determination when considering a semi-rigid molecule. To overcome these difficulties, powerful unsupervised techniques (such as machine learning algorithms) for the exploration of the degrees of freedom associated to the large amplitude motions are required.[143]

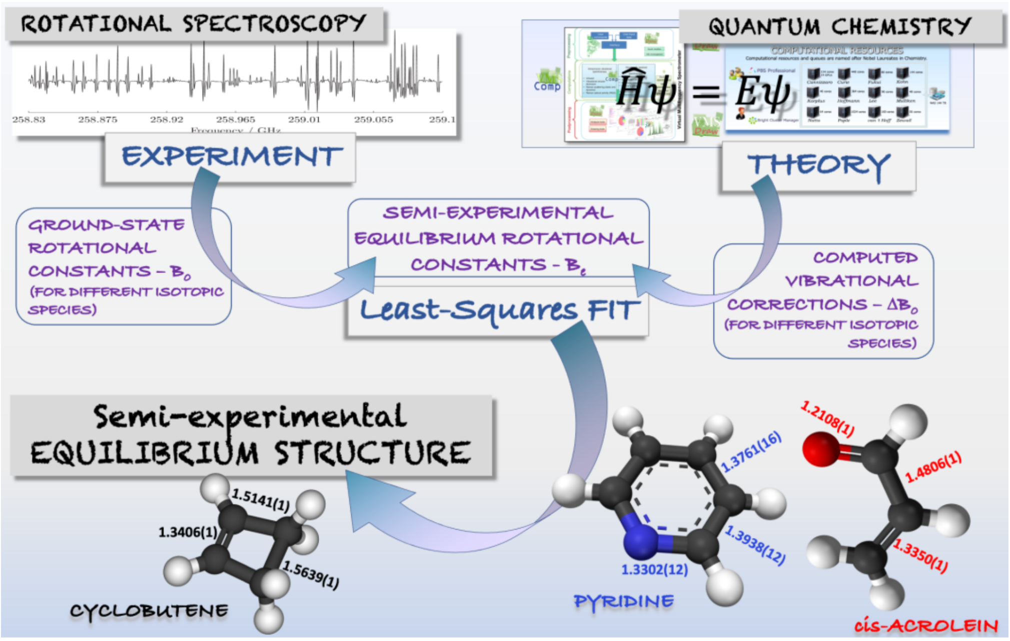

Figure 3. Schematic representation of the interplay of experiment and theory in rotational spectroscopy for the determination of molecular structure. Experimental vibrational ground-state rotational constants are computationally corrected for vibrational effects. The resulting semi-experimental equilibrium rotational constants for different isotopic species allow for the determination of the equilibrium structure.

[H2] 3.2. Vibrational/vibronic spectroscopy of flexible systems

The simplest approach to vibrational spectroscopy is based on the double harmonic approximation, which employs quadratic and linear approximations for the PES (for transition frequency) and PS (for intensity), respectively. This tool is available in several electronic structure QM codes, and it becomes extremely efficient whenever analytical energy second derivatives and property gradients are available. Mechanical (PES) and electric/magnetic (PS) anharmonicities can be introduced by means of perturbative[34,35,39-41,43] or variational[34,47,48,144-146] time-independent (TI) approaches. The first route, despite some limitations (e.g. the proper treatment of large amplitude motions, LAMs [G]), allows for a general and robust simulation of spectral line-shapes and vis-á-vis comparisons with experimental outcomes.[35,39-41,61] Integration of both models within a general platform simultaneously allows the correct treatment of small amplitude motions [G] (SAMs) and LAMs[142] Spectral simulation, analysis, and comparison with experiment can be greatly facilitated by dedicated graphical tools like, e.g., the Virtual Multifrequency Spectrometer (VMS).[61]

In TI models, structures and properties of energy minima and their local environments are employed in variational or perturbative formalisms mostly exploiting the Watson Hamiltonian[34] (given in Equation 3 and discussed in section 2.1). In time-dependent (TD) approaches, classical or semi-classical dynamics simulations are performed over the whole PES and the corresponding PS.[147-149] The two approaches (TI and TD) offer complementary information and the selection of the most appropriate strategy depends on several factors, including the environment (e.g. TI models are more suitable for isolated molecules and TD ones for condensed phases), the effective mass governing the motion (e.g. classical TD models are more effective for large masses), and other effects. For flexible molecular systems, harmonic models based on curvilinear coordinates[58] should be used; for systems with several low-lying conformers/tautomers, appropriate averaging of individual spectra must be performed. Analogously to rotational spectroscopy, the presence of several low-lying conformers/tautomers can tune the overall spectrum, thus requiring appropriate conformational searches and weighting of the spectra of the most stable structures by the corresponding Boltzmann populations.[150] In the case of solutions, for innocent solvents (that is solvents that do not establish specific interactions like, e.g., hydrogen bonds), solvatochromic effects can be incorporated at a negligible cost by means of the polarizable continuum model (PCM **[G]**)[34], while - in more complex cases - at least solvent molecules in the cybotactic **[G]** region must be explicitly included.[151]

Moving to vibronic spectroscopy, absorption or emission electronic spectra are the envelopes of specific vibrational levels of the initial and final electronic states. However, most of the current computations still employ rough phenomenological models in which vertical transition energies are broadened by empirical Gaussian or Lorentzian functions. Moreover, the analysis of experimental data is often based on the assumption that the peak maxima are related to the so-called 0-0 transition (transition between vibrational ground states of initial and final electronic state). However, it is impossible to know *a priori* which vibronic transition will be most intense, as it depends on the largest overlap of vibrational wavefunctions. Therefore, realistic simulations must take into account vibrational effects. In the Franck-Condon approximation the transition dipole moment (Eq. 11) is considered constant (i.e. nuclear-coordinate independent) in harmonic TI (sum-of-state)[52] or TD (path-integral)[53] approaches. The simplest formulation, based on one-dimensional vibrational overlaps between (a possibly reduced number of) identical normal modes for the different electronic states, is still employed in several studies and is also exploited in the prescreening procedure for more sophisticated TI computations.[51] While more accurate, direct nuclear dynamics simulations are prohibitive for large systems and, as such, the most advanced models employing highly accurate potential energy and property surfaces (PES and PS) can only be applied to small-sized molecules.[144-146] Integration of TI and TD models within a general platform allows at the same time simulations of highly resolved spectra (including band assignments) and full convergence of spectra at finite temperatures. For more complex, flexible systems several approximate yet sufficiently accurate approaches have been proposed[34,152-154] for both vibrational and vibrationally-resolved electronic spectra.

[H3] **3.2.1 The MI-IR spectrum of glycine**

A step-by-step route from the starting harmonic computations to the final realistic simulated spectra is presented in Figure 4 for glycine (H_2NCH_2COOH), the simplest amino acid. Glycine is characterized by conformational flexibility due to the rotation along three single bonds: N-C, C-C and C-O. The small size of the molecule allows for a full theoretical exploration of its conformational space, which confirmed the presence of eight local minima,[113,120,155] labelled by roman numbers referring to their stability order, with "p,n" describing the planarity or non-planarity of the backbone, and "c,g,t" the cis, gauche or trans orientation of the lone-pair(N)-N-C-C, N-C-C-O, and C-C-O-H dihedrals.

The six most stable conformers have been studied by means of Fourier transform infrared (FTIR) spectroscopy with three of them detected under the same experimental conditions.[156-158] Figure 4 compares the computed spectra with FTIR results for glycine deposited in a low-temperature matrix. The most intense experimental bands can be identified based on the harmonic spectrum of the most stable conformer Ip. An improvement (a more realistic spectrum) is obtained by including anharmonic corrections to band positions and intensities, with the consequent appearance of several new bands (non-fundamental transitions). The best agreement with experiment is obtained once the contributions from IIn and IIIp conformers, weighted for their Boltzmann populations, are added. Fully anharmonic spectra allow to distinguish between low-intensity bands related to non-fundamental transitions of the most abundant conformer (not present at harmonic level) and the fundamental transitions of the less abundant ones (see ref. [113] for detailed discussion and analysis).

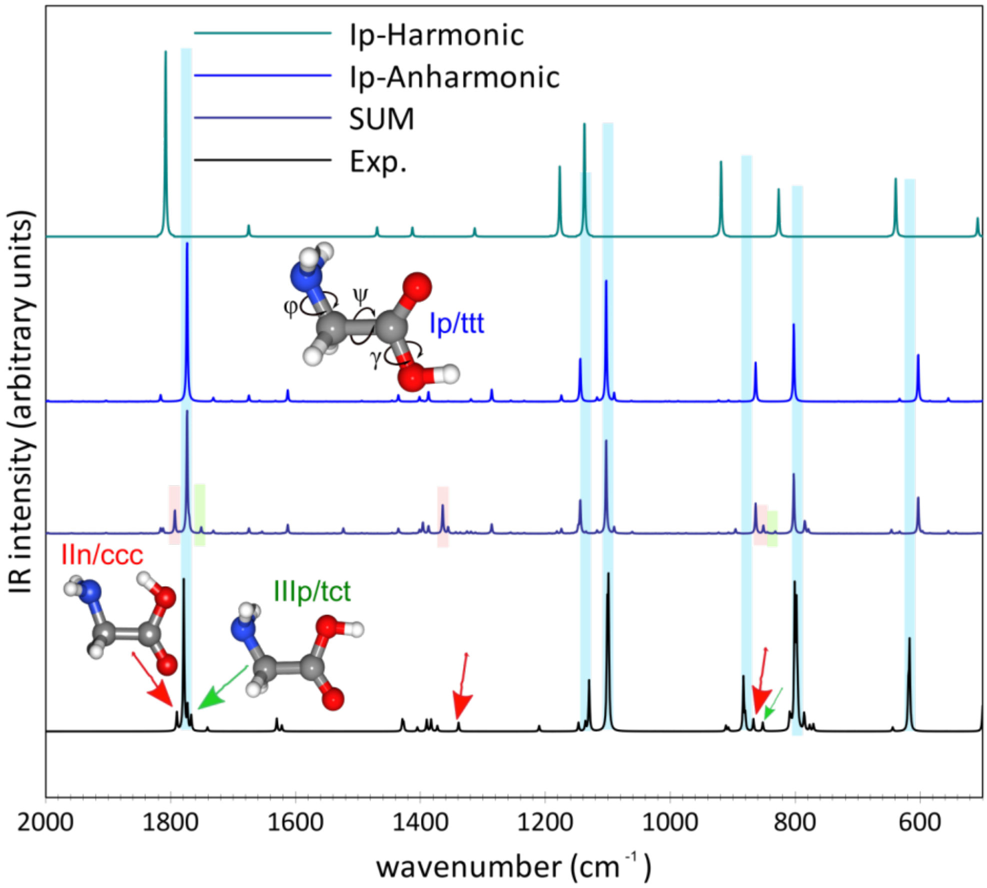

Figure 4. Computed[113] and experimental[157] MI-IR spectra of glycine. Simulated harmonic and anharmonic theoretical spectrum of the most stable Ip conformer together with the final spectrum resulting from the sum of the contributions of Ip/ttt, IIn/ccc and IIIp/tct conformers, weighted for their relative abundances, at 410 K (temperature of the sample preparation), also assuming the conformational cooling of less stable conformers.

[H3] **3.2.2 Vibronic spectrum of chlorophyll-a**

In general terms, vibronic spectra simulations are necessary to distinguish different contributions to the spectrum line-shape from different electronic transitions, conformers, or other species possibly present in the experimental mixture, for instance as photoproducts.[159] As an example, the UV-vis spectrum of chlorophyll-a in methanol solution (Figure 5) has been simulated considering environmental effects by means of hybrid implicit/explicit solvent model with the two methanol molecules coordinating the Mg ion and the bulk solvent effects accounted for using the PCM (see ref. [160] for the details, and ref. [135] for the gas-phase spectrum simulation).

The spectra of chlorophylls are traditionally described in terms of four bands, based on the simplified four-orbital Gouterman model:[161] two low-energy Q-bands and two high energy Soret (B) bands. The additional x/y labeling, according to the direction of their polarization within a macrocycle plane,[162] can also (as in this case) be used. The top panel demonstrates how the set of vibronic transitions defines the asymmetric shape of the lowest energy $S_1 \leftarrow S_0$ transition, which cannot be well described by the simplest vertical energy approach, irrespective of the applied broadening. This transition dominates the Qy band, but gives also a significant contribution to the Qx one. The final spectrum, which can be directly compared with the experimental one in the whole UV-vis range, is obtained from the single $S_x \leftarrow S_0$ (x=1-8) transition contributions. Simulation of vibronic spectra allows for the unequivocal assignment of the main spectral features, showing that the line shape is dominated by two pairs of overlapping transitions: $S_1 \leftarrow S_0$ and $S_2 \leftarrow S_0$ being the first pair and $S_3 \leftarrow S_0$ $S_4 \leftarrow S_0$ the second one. These pairs give rise to the Qy/Qx and By/Bx bands, respectively.

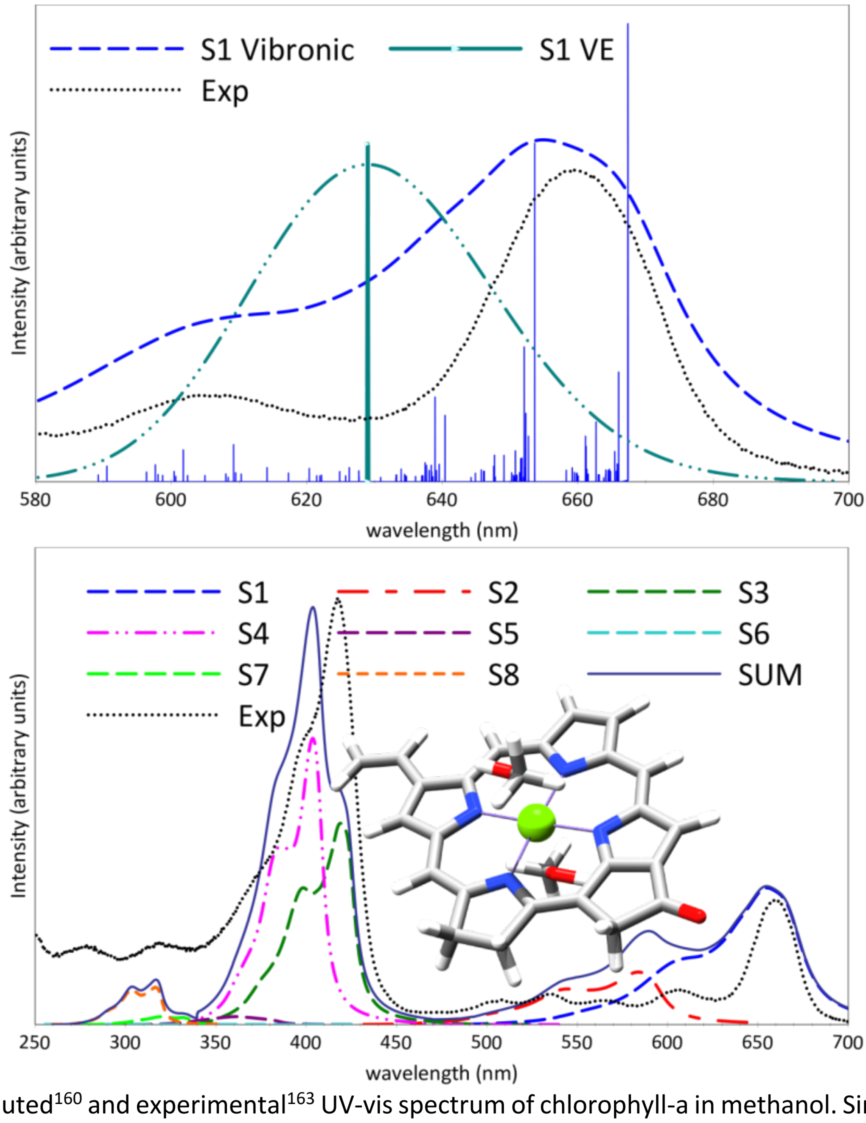

Figure 5. Computed[160] and experimental[163] UV-vis spectrum of chlorophyll-a in methanol. Simulated theoretical spectra: (top panel) $S_1 \leftarrow S_0$ (Q_y) transition simulated by the vertical approximation (VE) and vibronic spectrum; (bottom panel): absorption spectrum in the 250-700 nm range obtained as sum of vibronic spectra of the first 8 lowest single electronic transitions. All theoretical spectra are red-shifted by 450 cm^{-1} (about 20 nm). Theoretical stick spectra have been convoluted by Gaussian functions with a half-width at half maximum (HWHM) of 500cm^{-1} (VE) or Lorentzian functions with a HWHM of 250 cm^{-1} (Vibronic).

[H2] 3.3. Molecular vibrations from diffusion Monte Carlo

For molecules that undergo large amplitude vibrations, many insights can be obtained from knowledge of how the ground state wave function samples the potential surface, and how this is affected by isotopic substitution. DMC provides an approach that is well-suited to exploring ground state properties of molecules showing LAMs. The power of the DMC approach comes from the fact that the wave function is represented by an ensemble of localized functions (or walkers **[G]**) as described by Eq. (12). This allows for studies of systems that are not well-approximated by a simple zero-order (harmonic) description (like, e.g., torsions around simple bonds or ring puckerings). This comes at the cost that, generally, only one state can be calculated at a time, making the approach well-suited for studies that focus on the ground state wave function and associated properties including vibrationally averaged rotational constants.

In DMC, at each step in the simulation, a reference energy is evaluated using[86]

$$V_{ref} = \overline{V}(\tau) - \alpha\left(\frac{N_w(\tau)}{N_w(0)}\right) \qquad \text{(Equation 16)}$$

where the first term provides the ensemble average of the potential energy, and the second term adjusts the value of V_{ref} to ensure a nearly constant ensemble size throughout the simulation. Once the ensemble has equilibrated, the time averaged value of V_{ref} provides the zero-point energy of the system of interest.

It is important to recognize that this value fluctuates throughout the simulation, as is illustrated for $H^+(H_2O)_2$[164] in panels A-C in Figure 6. These plots show the evolution of V_{ref} for three different combinations of time increments ($\Delta\tau$) and ensemble sizes (N_w), where all simulations are propagated over the same total time. Generally, the size of the fluctuations of V_{ref} decreases as N_w or $\Delta\tau$ increases, thus improving the quality of the results, but also increasing the computational time. Additionally, the size of these fluctuations can be tuned by changing the value of α. For the plots shown in black in panels A-C of Figure 6, $\alpha = 0.5/\Delta\tau$. In panel C, we explore how the value of α affects the sizes of the fluctuations in V_{ref}. As is seen, when $\alpha = 0.5$, the fluctuations are largest, and as α is decreased to 0.1 or smaller, the size of these fluctuations remains roughly the same on the scale of this plot. On the other hand, if we focus on a smaller range of propagation times, we find that decreasing α removes the highest frequency fluctuations, while a low-frequency oscillation of V_{ref} remains (see lower panel of Supplementary Figure **2** in the Supplementary Information). In selecting α, one strives to identify a value where the high frequency oscillations of V_{ref} occur between roughly three and ten time steps. This choice lessens the correlation of V_{ref} between subsequent time steps without increasing the magnitude of the fluctuations of V_{ref}. Several tests confirmed that $\alpha = 0.5/\Delta\tau$ generally yields good results in this regard.[84,165,166]

The numbers shown in panel B provide the zero-point energy **[G]** that is obtained by averaging V_{ref} over different ranges of τ. The numbers in parentheses represent the standard deviation among five independent simulations that were performed using these parameters. As seen, the evaluated energy is relatively insensitive to how long the averaging is over, but the standard deviations are about half as large when V_{ref} is averaged over more than 10 000 a.u. of time. The evaluated zero-point energies for nine different combinations of ensemble sizes and time increments are compared in panel D. We note that the smallest N_w has the greatest uncertainty in its zero-point energy, and when one uses both the smallest N_w and the largest $\Delta\tau$, the simulation yields a zero-point energy that is inconsistent with the benchmark calculation (dotted line with grey shading). The larger ensembles provide zero-point energies that agree with the benchmark results for all three time increments. However, as with the fluctuations of V_{ref}, the statistical uncertainties in the reported zero-point energies decrease for smaller $\Delta\tau$ and for larger ensembles, so a compromise must be made between accuracy and computational time.

In addition to the zero-point energies, DMC provides a powerful tool for obtaining projections of the ground state probability amplitude onto a desired coordinate. This is achieved by propagating the ensemble of walkers over a short period of imaginary time **[G]**, τ_{DW}, and identifying the fraction of the ensemble at $\tau + \tau_{DW}$ that is traced to a particular walker in the ensemble at τ. This number is proportional to the value of the wave function at the coordinates of the walker at τ,[84,87] allowing us to use Monte Carlo integration to generate the desired projection of the probability amplitude, Ψ^2. This approach is used to obtain the projection of the ground state probability amplitude onto the Δr (see inset in panel E), and the resulting distributions are shown in the panel E of Figure R4 for several values of τ_{DW}. As it is hard to differentiate among these results, the mean values of Δr, along with the standard deviation, are shown as functions of τ_{DW} in panel F. The convergence of the results can be estimated by the results reported in this panel, which compares the computed values against independently obtained values of these quantities based on symmetry ($\langle \Delta r \rangle$, black dotted line) or an alternative way to obtain expectation values ($\sigma_{\Delta r}$, green dotted line).[83,167]

Extensions to DMC that enable the study of excited state energies and wave functions have been developed,[86,168-170] although a discussion of these is beyond the scope of the present Primer.

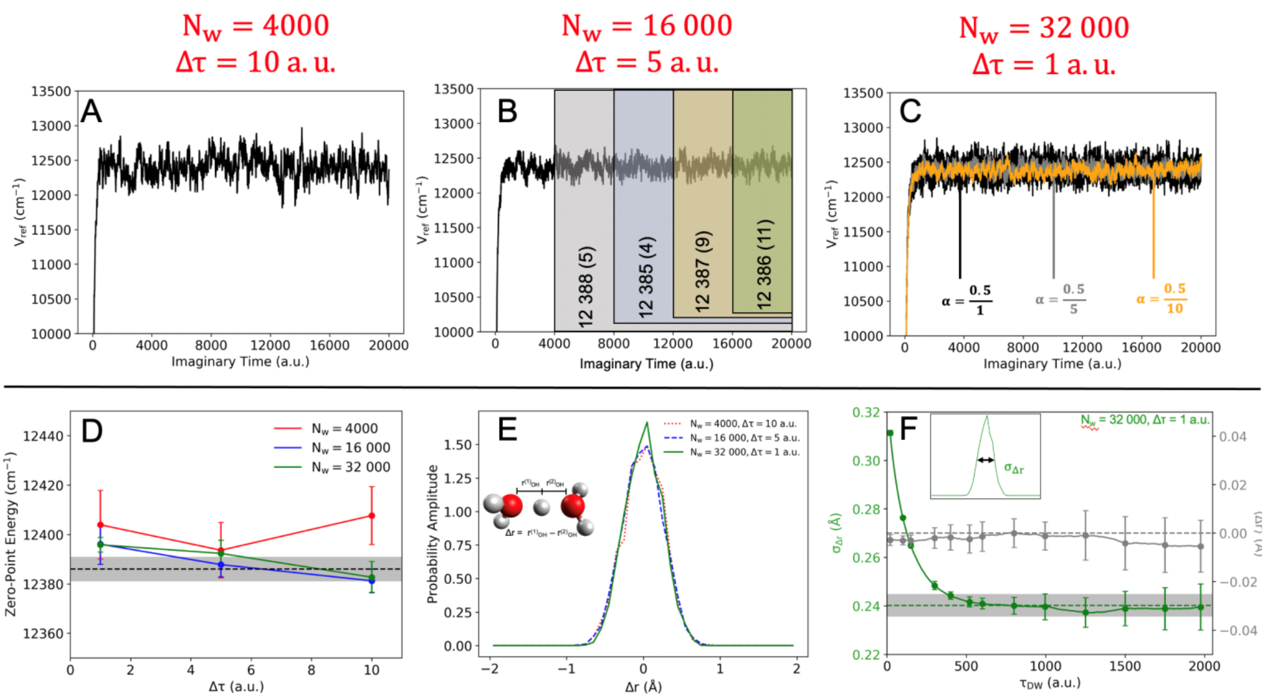

Figure 6: (A)-(C) The value of V_{ref} plotted as a function of imaginary time, obtained from DMC simulations using (A) N_w=4000 and $\Delta\tau$=10 a.u.; (B) N_w = 16 000 and $\Delta\tau$=5 a.u.; and (C) N_w = 32 000 and $\Delta\tau$=1 a.u.. In panel B, we also show how the evaluated zero-point energy depends on how long V_{ref} is averaged. These values are also tabulated in the Supplementary Information (Supplementary Tables **1** to **3**). In Panel C, we also explore how the size of the α-parameter (see equation above) affects the magnitude of the fluctuations in V_{ref}. (D) The calculated zero-point energy is plotted as a function of the time increment for ensemble sizes ranging from 4000 (red) to 3200 (green) walkers, and compared to the results obtained using N_w = 20 000 and a time increment of 10 a.u. (black line, where grey shading indicates a 5 cm^{-1} uncertainty in that value). (E) Projections of Ψ^2 onto Δr (see inset) as a function of ensemble size based on a calculation where the number of descendants is evaluated after τ_{DW} = 520 a.u. (F) The expectation value (grey) and standard deviation of Δr , plotted as a function of τ_{DW}. The dotted grey and green lines provide reference values of 0 Å for the average and 0.240 Å for the standard deviation. While the average value of of Δr can be determined by symmetry, the standard deviation is obtained using an adiabatic DMC calculation.[83,167] All error bars and uncertainties reflect the standard deviations among five independent DMC simulations.

[H2] 3.4. Determination of absolute configurations

The chiral spectroscopic techniques considered here (ORD, ECD, VCD and ROA) play a fundamental role in the determination of absolute configuration (AC) **[G]**. As spectra for enantiomers are mirror images, the AC can be determined by comparing the calculated spectra with the experimental ones. In the simplest case, in order to determine the AC using the methods mentioned above, the spectra of the two enantiomers are calculated and compared to the experimental spectrum of one of the enantiomers, (+) or (–). The calculated spectrum in best agreement with the experimental spectrum defines the AC of the experimental enantiomer. As an example, the experimental and calculated VCD spectra for (+)-camphor and (1R,4R)-camphor are shown in Figure 7a. Given the quantitative agreement between the calculated and experimental spectra, the AC of (+)-camphor is assigned to be 1R,4R. Since these are enantiomers, it follows that (-)-camphor is (1S,4S).

Each of these chiral spectroscopies can be applied individually or in combination.[171-176] The advantage of using multiple methods is that they provide complementary information, which is useful in distinguishing diastereomers with multiple chiral centers, as one method may not be able to distinguish particular stereocenters. Specifically, Polavarapu et al.[171] found that ORD, ECD and VCD were individually unable to unambiguously assign the AC of Hibiscus and Garcinia acids, each containing two chiral centers. However, a combination of VCD with either ECD or ORD was able to correctly assign the AC of both molecules. Similarly, Hopman et al.[176] found that VCD and ROA, but not ECD, were able to correctly assign the AC of Synoxazolidinone, a marine antibiotic compound containing two chiral centers and one asymmetrically substituted double bond, resulting in a total of eight possible stereoisomers. A recent study by Bogaerts et al.[174] on Artemisinin, an anti-malaria drug containing seven chiral centers, found that even though ROA and VCD could independently assign the correct stereochemistry, the combination of these two methods resulted in an even stronger unambiguous AC assignment (VCD and ROA spectra shown in Figure 7b,d).

For molecules containing multiple chiral centers and whose diastereomers predict similar spectra, the harmonic approximation, which is routinely used for VCD and ROA, may not be sufficient in providing a reliable AC assignment. This is the case for Diplopyrone, a phytotoxic monosubstituted tetrahydropyranpyran-2-one, containing four chiral centers, two of which were previously unassigned.[173] In addition, this molecule possesses several low-energy conformers, further complicating the analysis of the spectra as discussed in section 3.2. In this case, ECD was not able to distinguish between the four possible diastereomers and the diastereomers predicted very similar harmonic VCD spectra. However, VCD spectra computed at the anharmonic level (Figure 7f) were sufficiently close to experiment to allow for a confident assignment of the two unknown chiral centers.

The comparison of calculated and experimental spectra is an important part of the assignment of AC. Although this comparison can be performed visually, different approaches exist to remove bias and to quantify the degree of similarity. All of these methods rely on the calculation of a spectral overlap between the experimental and predicted spectra.[172,174] Another approach involves the analysis of the dissymmetry factor, the ratio of $\Delta\epsilon$ and ϵ.[69,175,177] Another measure of the reliability of the calculated vibrational spectra is the concept of robust modes, first developed for VCD[178] and later extended to ROA.[179] In this approach, a mode is determined to be robust if the rotational strength or scattering activity will not change sign due to small perturbations in either experiment or calculation.

Although the primary utility of the chiroptical vibrational methods is to produce the spectra shown in Figure 7, additional information can be extracted which can help in the analysis and interpretation of the results. These include examining the vibrational transition current density associated with a molecular vibration[180,181] for VCD and computing atomic contribution patterns and group coupling matrices[182] for ROA.

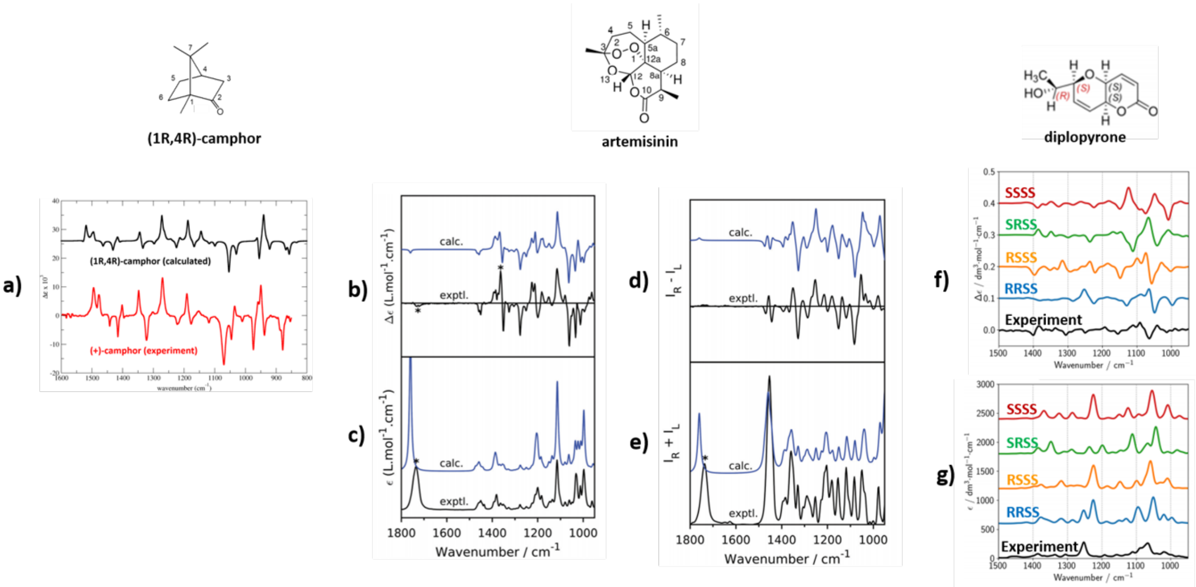

Figure 7: Computed and experimental VCD and ROA spectra for the determination of AC. (a) Comparison of calculated and experimental VCD spectra for (1R,4R)-camphor and (+)-camphor, respectively. Calculated spectra are plotted using the Lorentzian lineshape function using a HWHM of 4 cm^1. Experimental data, originally from ref [66], kindly provided by Frank Devlin (USC). (b-e) Comparison of calculated and experimental VCD (b) and IR (c) and ROA (d) and Raman (e) spectra for artemisinin. Calculated spectra are plotted using the Lorentzian lineshape function using a HWHM of 5 cm^{-1} for VCD/IR and 8 cm^{-1} for ROA/Raman. Figure taken from [176]. For a molecule containing seven chiral centers there would, in principle, be $2^7 = 128$ diastereomers, but since two of the chiral centers are fixed (via the endoperoxide bridge) this number is reduced to $2^6 = 64$. However, half of these are enantiomers so that conformational analysis and spectra calculations were performed for a total of 32 diastereomers. (f-g). Comparison of calculated anharmonic and experimental VCD (f) and IR (g) spectra for (+)-diplopyrone ((+)-6-[(1R)-1-hydroxyethyl] 2,4a(S),6(S),8a(S) tetrahydropyran[3,2-b]pyran-2-one). Calculated spectra are plotted using the Lorentzian lineshape function, using a HWHM of 8 cm^{-1}. Figure taken from [173].

[H1] 4. Applications

As done for the results section, a limited selection of possible applications is reported to provide significant examples of the potential of computational molecular spectroscopy, the examples being selected from the spectroscopies addressed in this Primer. However, the list of possible applications is too long for being even simply enumerated here.

[H2] 4.1. Astrochemistry

The role of spectroscopic techniques in the study of the interstellar medium (ISM) has grown rapidly in the last few decades, with rotational spectroscopy playing a critical role. Most of the understanding of the ISM – the gas and dust existing in the space between the stars of a galaxy – comes from Earth-based spectroscopic observations. Atoms and molecules in the gas phase constitute 99% of the ISM's mass, while the remaining mass is composed of silicate and carbonate grains.[183] At the low temperatures of the ISM, gas-phase particles emit radiation whose frequency spans from the gigahertz to the terahertz domains. Physically, the quanta emitted corresponds to the transitions between rotational energy levels of molecules. Thus, each molecule can be identified through its peculiar fingerprints - i.e., its rotational transitions.[183] With these molecules being ubiquitous in the ISM, the chemical composition - as well as the physical properties and the evolutionary stage of interstellar objects - can be derived from radioastronomical observations.[184] The laboratory data needed to guide the latter and to discover new interstellar species are provided by rotational-spectroscopy laboratory studies,[185] which are increasingly supported and complemented by QC computations.[140]

The search for interstellar complex organic molecules (i-COMs, i.e. species containing at least six atoms and composed of carbon, hydrogen, oxygen, and/or nitrogen[186] can be assisted by the Minimum Energy Principle (MEP), which states that "the most stable isomer of a given chemical formula is always the most abundant in the ISM".[187] A computational study of the relative stability of different isomeric (structural or conformational) species allows the screening of potentially observable molecules. In the case of conformers, the energy difference among the various conformers can be as small as a few kJ/mol, and the size of the electric dipole moment becomes an important parameter worth computing (the intensity of rotational transitions scales with the square of the dipole moment component that allows the transition). The combination of the MEP and the magnitude of the electric dipole moment enables the straightforward identification of the most likely detectable i-COMs.

Once the species of interest is recognized, computational spectroscopy guides the experimental study by providing accurate predictions of the rotational parameters to be used for simulating their spectra.[141,188] Despite the potential accuracy that can be reached by such calculations,[140] this is generally insufficient for directly guiding astronomical searches and/or assignments. However, in some cases, QC predictions can assess the detection of new astrochemical species, as is the case with the cyanobutadiynyl anion, C_5N^-.[189] Due to the difficulty of producing this species, no laboratory study of its rotational spectrum has been reported to date. Nonetheless, C_5N^- has been discovered in the envelope of a carbon-rich star thanks to the pinpoint match between astronomical observations and predictions based on high-level coupled-cluster calculations.[190]

The analysis of astronomical spectra can provide new information; however, the help of QC calculations is often needed. To give a specific example, the investigation of the hyperfine structure of the rotational spectrum is fundamental to gaining information on column densities, which provide a measure for molecular abundances. The hyperfine structure in rotational spectra is due to interactions between the molecular electric and/or magnetic fields and the nuclear moments. The most important of these interactions is that between the molecular electric-field gradient and the electric quadrupole moment of nuclei (with the latter being present when the nuclear spin is greater than 1/2). Among the magnetic interactions, the weak magnetic field generated by the end-over-end rotation of a molecule interacts with the nuclear magnetic moments, thus producing a slight magnetic split or shift of the lines (with nuclear magnetic moments being present when the nuclear spin is non-null). These two interactions are referred to as nuclear quadrupole coupling and spin-rotation interaction, respectively; in addition, dipolar spin-spin interactions among different nuclear spins may also arise. In the case of molecular ions, the resolution of experiment is usually limited by the impossibility of reducing the working pressure inside the cell (because of the ion-production process),[191] thus leading to the partial or even non-resolution of hyperfine structures, as shown in Figure 8. Interstellar lines are instead very narrow. Therefore, when required, one can resort to QC calculations to accurately predict the hyperfine structure of astronomical spectra: the quantitative accuracy obtainable with state-of-the-art QC calculations is demonstrated in Figure 8. Another significant example is offered by CF^+,[192] for which the hyperfine structure of the astronomical (rotational) spectrum was assigned using the computed hyperfine parameters.

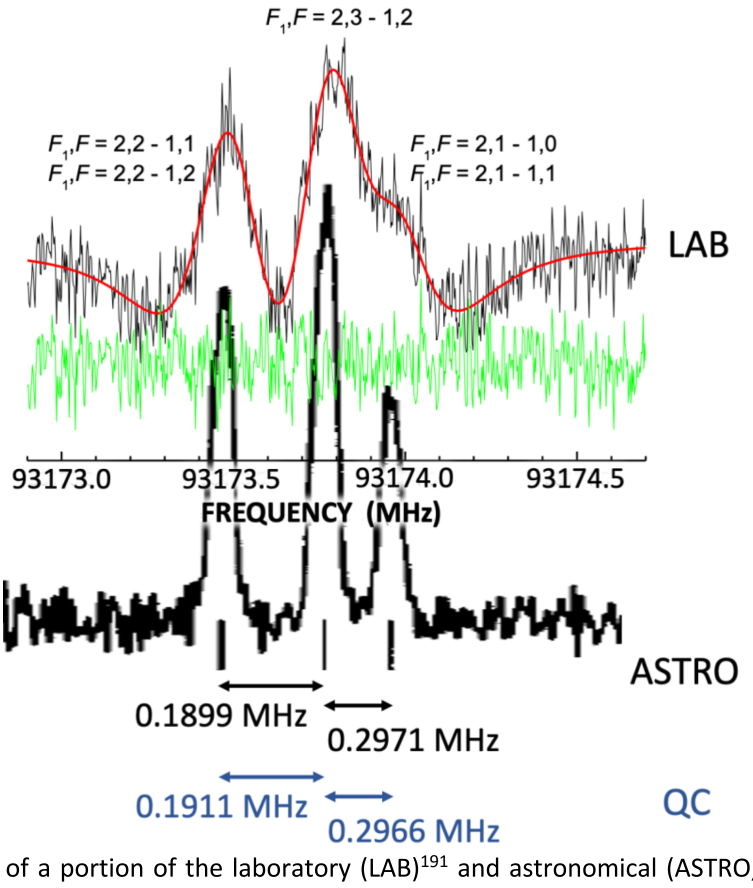

Figure 8. Comparison of a portion of the laboratory (LAB)[191] and astronomical (ASTRO, low-mass cloud core L1512 in Taurus[193]) spectrum of the first rotational transition (J = 1 – 0, with J being the rotational quantum number) of the diazenylium cation (N_2H^+). The actual comparison is between the red LAB spectrum (resulting from the line profile analysis of recorded spectrum in black, with the green trace being the corresponding residual) and the ASTRO counterpart, with the hyperfine splittings also reported. These are compared with the computed (QC) values.

The hyperfine structure is due to the presence of two nuclear quadrupolar nuclei, the nitrogens. The quantum numbers F_1 and F arise from the coupling schemes $\boldsymbol{F}_1 = \boldsymbol{J} + \boldsymbol{I}_{N1}$ and $\boldsymbol{F} = \boldsymbol{F}_1 + \boldsymbol{I}_{N2}$, respectively, with $\boldsymbol{I}$ being the nuclear spin quantum number (=1 for nitrogen).

Finally, an appropriate modeling of the ISM demands the computation of collisional rate coefficients for interstellar molecules by the most abundant species, i.e. hydrogen and helium (denoted as collider). Interstellar species are often far from a local thermodynamic equilibrium (LTE) condition. Therefore, the collisions occurring between the molecule under consideration and molecular hydrogen (or atomic helium) significantly affect the population of rotational levels of the former and thus have an impact on the rotational transitions observed with radioastronomy.[194] In turn, the derivation of collisional data requires the computation of the PES of the molecule-collider with high accuracy.

[H2] 4.2. Weakly bound clusters and biomolecules

A wide and expanding application of computational spectroscopy is the calculation of spectra for weakly bound clusters and biomolecules. In its broadest sense this includes magnetic and electronic spectroscopy[195,196] but here we will confine comments to vibrational spectroscopy with applications mainly to the near and far infrared region of the spectrum.

Advances in high resolution infrared spectroscopy of small van der Waals molecules have stimulated very good agreement between theory and experiment.[197] This work started with rare gas atoms attached to diatomic molecules[198] but has been extended to larger weakly bound clusters involving polyatomic molecules[199]. Clusters involving water molecules have received particular attention due to the importance of water throughout the sciences.[200] Water dimer is a key system and highly accurate fully dimensional potential energy surfaces have been produced from sophisticated *ab initio* procedures.[201] These potentials have been used in converged calculations of vibrational states using appropriate basis functions for the different degrees of freedom and full-dimensional Hamiltonians with variational procedures. This has led to excellent agreement between theory and experiment for the spectra in the far infrared region of the water dimer.[202]

This advance is important as the PES for water dimer forms the main component of potentials for larger water clusters, as the only supplements needed are fairly simple three- and four-body interactions between the different water molecules.[203] More challenging is the accurate calculation of the ro-vibrational states of water clusters larger than the dimer, as conventional basis set methods with variational procedures then quickly become unwieldy. However, alternative procedures have been applied for larger water clusters that can calculate quite accurately some parameters of experimental interest, such as the rotational constants of the lowest vibrational states of clusters of different geometries, and tunneling splittings of vibrational states arising from identical minima on the potential energy surfaces. In this way diffusion DMC,[204-206] instanton,[207] and path integral[208] procedures have been applied effectively on clusters up to $(H_2O)_8$ and have allowed detailed comparison with far infrared and microwave experiments.

The general importance of water in biology has meant that clusters of water with molecules of biological interest have been the subject of numerous calculations.[209] Methods such as DMC can also be applied to calculate structures of geometric isomers of biomolecules and the associated rotational constants.[210] QC calculations of infrared spectra for complexes such as uracil-water have shown the importance of hydrogen bonding and anharmonic effects in these systems.[211]

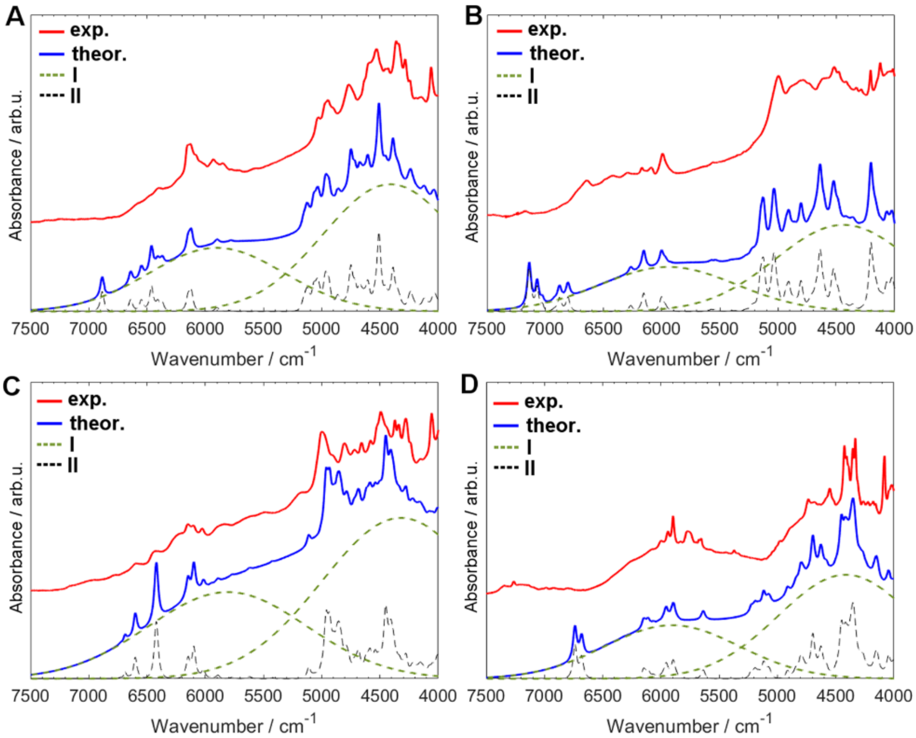

Figure 9. Experimental and calculated near infrared spectra of crystalline (A) adenine; (B) cytosine; (C) guanine; (D) thymine in the 4000–7500 cm^{-1} region.[212]

For more complicated biomolecules the whole plethora of quantum chemistry, DFT and more approximate procedures such as QM/MM and semiempirical force fields have been applied.[213] In the simplest approaches just the harmonic frequencies are calculated but anharmonic aspects have also been considered using a variety of quantum mechanical (QM) procedures including VPT2 and VSCF.[214]

A good example of a recent study is a calculation[212] of the near infrared spectra of the crystalline structures of DNA bases in which results from Deperturbed VPT2 (DVPT2) calculations were compared in detail with experiment (see Figure 9). Calculations such as those shown in Figure 9 demonstrate the power of computations in predicting and interpreting the vibrational spectra of molecules of biological interest. Indeed, assignment of the different overtones and combination bands found in this high-energy region (4000-7500 cm^{-1}) and their interpretation in terms of structural motifs would be very difficult (and questionable) without the help of QC computations.

[H2] 4.3. Spectroscopy of d- and f-elements

The spectroscopy of *d*- and *f*-elements introduces new experimental and theoretical challenges that are not easily met. At the heart of the challenges associated with these elements is the fact that they can exist in a variety of oxidation states that lead to spectroscopically well-defined d^n and f^n configurations (*n*=number of electrons in the *d*- or *f*-shell).

Given the high effective nuclear charge experienced by the *d*- or *f*-electrons, the corresponding orbitals are compact. Hence, compared to the strong bonds formed between main group elements, the *d*- and *f*-elements bind comparatively weakly through their orbitals to the surrounding ligands. Thus, the ligand environment induces limited orbital splittings **[G]**. This has been exploited very fruitfully in the phenomenological model of crystal field theory **[G]** (CFT[215]). In CFT, the *d*- or *f*-electrons are treated as free ions perturbed by an electrostatic field created by the surrounding ligands. While quantitatively unrealistic, the theory captures essentials of *d*-(*f*-) element electronic structure. Thus, the combination of a partially filled *d*- or *f*-shell and limited ligand field splittings leads to a series of low-lying electronic states formed from distributing *n*-electrons between the available orbitals and at the same time couples their spins in all possible ways to a resulting net total spin. On top of the complexity arising from a large variety of multiplets **[G]** comes the fact that *d*- and *f*-elements are heavy. Hence, the effects of relativity become much more prominent in these compounds and whenever there are unpaired electrons, a treatment of the spin-orbit-coupling (SOC **[G]**) becomes mandatory for theoretical spectroscopy.[13] The electronic complexity is necessarily also reflected in the observed spectra. Throughout the range of available techniques ranging from hard X-rays (10^4 eV) down to microwaves and radiowaves (10^{-11}-10^{-9} eV)) the spectra typically show a high amount of spectral crowding due to the multitude of final states that can be reached in the respective spectroscopic transitions. In addition, the spectra are difficult to interpret because of the complexity of the electronic states that are involved and consequently, they require a high amount of expertise to be interpreted correctly.

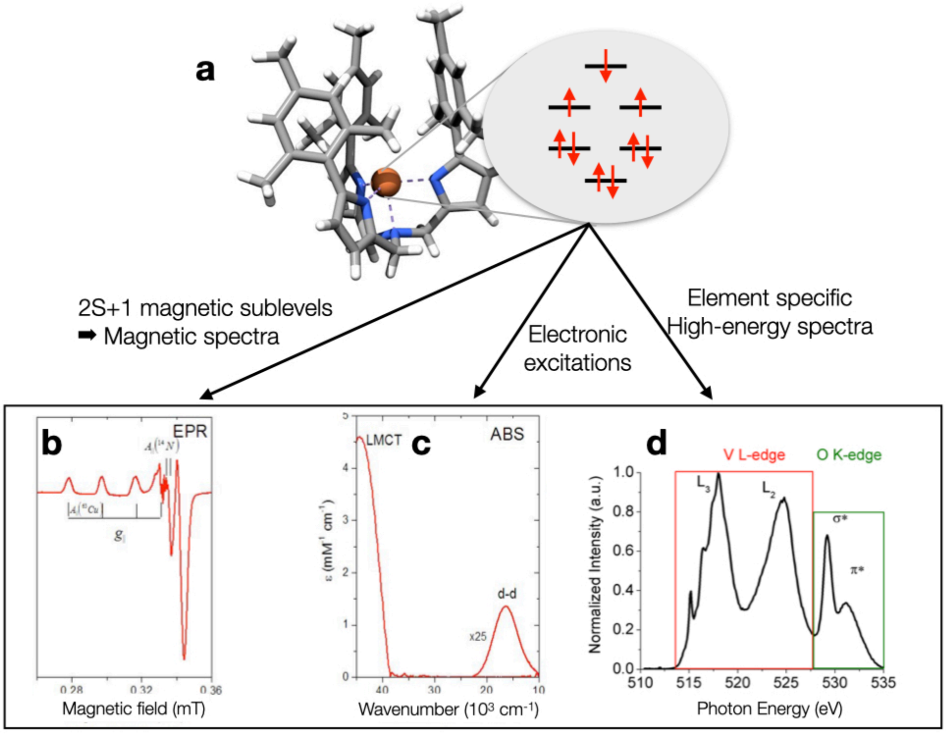

Figure 10. The complex arrangements of electrons in partially filled *d*- and *f*-shells give rise to a wide variety of spectroscopic phenomena that are challenging to model with high-accuracy by quantum chemistry. The geometric structure (panel **a**: left, grey=carbon, white=hydrogen, blue nitrogen, brown=transition metal) imposes a distinctive splitting of the molecular orbitals that are based on the transition metal d-orbitals (panel **a**: right). The distribution of the n electrons in a d^n configuration gives rise to a multitude of electronic states that can be probed with optical or magnetic spectroscopy (panels **b**-**d**). Among these, the most prominent ones are EPR (**b**), absorption (**c**) and X-ray absorption (**d**) spectra. EPR spectroscopy probes the net electron spin caused by the unpaired electrons of the electronic ground state. ABS probes transitions of electrons between valence orbitals, including the metal d-based orbitals. X-ray spectroscopy probes excitations from deep core electrons on the transition metal center(s) into the empty or half-filled valence orbitals. Since the core levels vary systematically along the periodic table, this provides a highly sensitive element specific probe of the system under investigation.

The complex electronic multiplets in the presence of relativistic effects are not easily reproduced even in a semi-quantitative way by the available QC methods.[216-218] In those cases where there are (near-) orbital degeneracies (as readily predicted by CFT), there may not be a single Slater determinant **[G]** that is an appropriate starting point for the description of the electronic ground state. In such a case, all single-reference determinant based methods (including DFT) fail to describe the electronic structure of either the ground or the excited states correctly. Typically, not even the number of reachable final states tend to be correct.[13,17] Thus, DFT has many serious shortcomings in the field of theoretical *d*- and *f*-element theoretical spectroscopy. These shortcomings were highlighted in some reviews over a decade ago and stand unchanged today.[13,17,219]

The occurrence of a rich multiplet structure together with the prominence of relativistic effects, opens up rich opportunities for experimental spectroscopy (Figure 10). Magnetic low-energy spectroscopies, such as NMR and ESR, can probe the magnetic sublevels of the electronic ground state multiplets, while modern magnetometry is extensively used to study the magnetic properties of *d*- and *f*-elements for molecular magnetism. Electronic spectroscopies including UV/vis, CD and magnetic CD (MCD **[G]**) or resonance Raman spectroscopies provide in-depth insights into the electronic structure of these species. Finally, since there are typically only a few atoms of a given element present in the compound, element specific techniques like Mössbauer or X-ray absorption/emission spectroscopies are very widely used.[17] All of these methods provide detailed fingerprints of the geometric and electronic structure of the systems under investigation. Importantly, each one of these techniques is sensitive to different geometric and electronic structure details. Thus, there is a host of experimentally available electronic structure information. However, in order to develop the full information content of these spectra, it is inevitable to turn to quantum chemistry for spectral interpretations. A successfully carried out study results in experimentally calibrated electronic structure level insight of the investigated species, be they stable entities or reaction intermediates. As discussed elsewhere, this leads to insights that can not be obtained from the pure calculation of total energies[220,221]

[H3] **4.3.1. Case study of magnetic Co(II) tetrathiolates**

Coordination complexes of Co(II) ions (d^7 configuration) have been known in coordination chemistry since its cradle days and have been routinely characterized with magnetic measurements like SQUID **[G]**, EPR or MCD spectroscopy. It is well-known that in an approximately tetrahedral environment the ground state has a total spin of S=3/2. A cursory look at the ion $[Co(S\text{-}Ph)_4]^{2-}$ also reveals nothing particularly special. However, this changed dramatically when Long and coworkers reported that this ion show slow magnetic relaxation at zero magnetic field. This is the signature of the very thought-after single-molecule magnet (SMM) behaviour.[222] What is particularly exciting is that $[Co(S\text{-}Ph)_4]^{2-}$ was the first mononuclear compound to show this behavior where for several decades it was believed that only large, oligonuclear transition metal clusters could show SMM properties (see[223]).

A careful study of the magnetic properties of two different salts containing $[Co(S\text{-}Ph)_4]^{2-}$ coupled to quantum chemical calculations were subsequently reported.[224,225] Quite surprisingly, only the $[Co(S\text{-}Ph)_4](P(Ph)_4)_2$ was showing SMM behavior, while $[Co(S\text{-}Ph)_4](N(Et)_4)_2$ did not. The careful experimental investigation showed that this is due to the Co(II) ion $P(Ph)_4$ having a large and negative zero-field splitting (ZFS **[G]**), while in the $N(Et)_4$ salt, the ZFS is small and positive. The magnetic properties of both structures were reproduced with excellent accuracy through CASSCF/NEVPT2 calculation with inclusion of spin-orbit coupling (SOC). Furthermore, the method of Ab Initio Ligand Field Theory (AILFT **[G]**) allowed for the ligand field parameters to be deduced from the large-scale wavefunction based ab initio calculations. They revealed that the origin of the radically different behavior is a subtle distortion that renders Co(II)-ion in the $P(Ph)_4$ salt to be in an elongated tetrahedral environment, while in the $N(Et)_4$ salt, it is in a compressed tetrahedral structure. The changes in the d-orbital splitting pattern are then sufficient to cause the dramatic switch of magnetic properties, as predicted by ligand field theory. Quite fascinatingly, the origin of the dramatically different behavior can thus be traced back to weak intermolecular interactions in the second coordination sphere of the cobalt. These insights opened up the avenue for many further investigations on Co(II) complexes (e.g. [226]). This study (summarized in Figure 11) is one demonstration that a large body of complex and initially puzzling experimental observations can be quantitatively interpreted in a unified manner through large-scale multireference *ab initio* calculations. Moreover, the results of these calculations can be translated concisely into a familiar chemical language through the AILFT procedure.

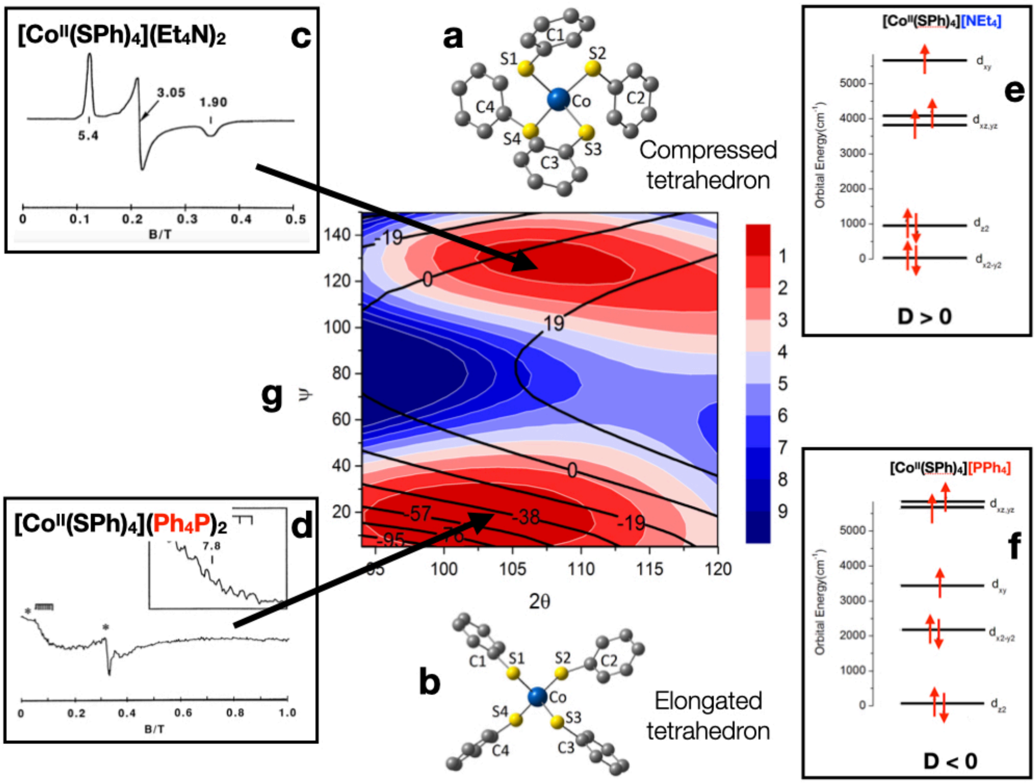

Figure 11. Panels **a,b**: the two structures of $[Co(S\text{-}Ph)_4]^{2-}$ found in the $(Et_4N)_2$ and $(Ph_4P)_2$ salts reflecting compressed and elongated tetrahedra respectively. Panels **c,d**: the radically different EPR spectra of the two species demonstrating their very different electronic structures. Panels **e,f**: the effective d-orbital splitting patterns deduced from CASSCF/NEVPT2 calculations for the two structures effectively explaining the origin of the very different D-values. Panel **g**: Potential energy and property surface (ZFS-value) for two key angles describing the distortion into flattened and elongated tetrahedra in $[Co(S\text{-}Ph)_4]^{2-}$. There are two shallow minima associated with qualitatively different D-values as reflected in their ESR spectra (**a,b**) and readily understood from quantum chemical calculations (**c,d**).

[H1] 5. Reproducibility and data deposition

Here we discuss different levels at which the issue of data reproducibility and deposition can be examined.

The first level is the definition of a general standard for the inputs and outputs (I/O) of electronic structure codes; this was discussed, for instance, in the MOLSSI workshop (https://molssi.org/2019/08/19/molssi-workshop-rovibrational-molecular-spectroscopy/). Indeed, we have been witnessing an increasing number of large-scale international and interdisciplinary collaborations, which often involve shared infrastructures and multi-user facilities, resulting in massive amounts of data. To enhance these collaborations, there is a strong need to integrate and standardize computational codes starting from a common syntax and/or language. An example in this direction is provided by the VMS project,[61] which aims at integrating several spectroscopic techniques and providing a user-friendly interface to different QC programs (see, e.g., the module dedicated to rotational spectroscopy[142]).

The second level is the compilation and management of highly accurate results for small (2-4 atoms) molecules, which can rival the corresponding experimental data.[34] Outside this narrow size range, theoretical models and computational procedures for computational spectroscopy are always based on approximations and assumptions, which need to be correctly recognized in the applications to realistic systems. Thus, small molecules can represent suitable fragments for benchmarking less refined methods and defining transferable correction factors for fragments of larger molecules.[227] The latter paves the way toward the set-up of public databases of molecular structures and spectroscopic properties. One example is provided by the database of semi-experimental equilibrium structures (derived as described in section 3.1) available at https://smart.sns.it/molecules/.

The third level concerns the lines to be followed for the spectroscopic characterization of large systems, which are of increasing interest to different scientific communities. The available results for an adequate number of medium-sized systems should be organized in sets of comparable accuracy by clustering techniques employing widely accepted general criteria. For some properties (essentially energies), the general definition of platinum, gold and silver standards[228] is more or less accepted. These definitions are based on the accuracy provided. For example, CCSD(T) calculations extrapolated to the complete basis set limit define the gold standard. The silver standard provides the best approximation to the gold standard at a reduced computational cost, while the platinum standard improves the gold one by adding further corrections (such as higher-order coupled cluster terms). However, such standards have not been developed for most spectroscopic properties, and for them the situation is thus more challenging. For instance, fully quantitative results for high-resolution spectroscopic techniques like rotational spectroscopy are still out of reach even for semi-rigid tri- and tetra-atomic systems,[229] the required computations being unaffordable. However, new methods based on the template approach **[G]** possibly coupled with the machine-learning appear quite promising.[227,230] To give an example, in the field of vibrational spectroscopies, some methodologies (such as VPT2 treatments based on an anharmonic description of the PES at a suitable level of theory[34]) can reach an accuracy within 10 cm^{-1} and are also applicable to large-sized systems with the help of linear scaling[231,232] and reduced dimensionality[233] techniques. In this connection, the compilation and management of databases (as mentioned for the second level for large molecules) is a task of current interest in the field. More work in this direction should be performed with compilations of spectroscopic parameters for molecules including heavy elements and for different spectroscopies. The situation is instead more involved for spectroscopic transition intensities, where the definition of widely accepted standards is still missing. Another important issue when dealing with large systems is their flexibility, which requires the implementation of effective approaches to search for the energetically low-lying structures (i.e. conformers or isomers).[150] In fact, a key point toward data/spectra reproducibility is the understanding of which of these conformers or isomers contribute to the overall spectroscopic signal. However, we are still far from any general definition of classes of methods/models achieving a desired accuracy.

Focusing on an integration of the levels 2 and 3, an interesting option would be to simulate and store overall spectra in place of databases collecting lists of spectroscopic parameters. Another step forward would be the set-up of compilations that combine results of different spectroscopies having comparable accuracies in view of their use to assist the experimental work, which more and more rests on the integrated use of different techniques.

A transversal issue is the role of environmental effects (e.g. solvent), which should be analyzed for different properties and/or solvents, thus allowing for the use of the most appropriate model for the specific case under consideration. Indeed, when the spectroscopic investigation is carried out in solution or, more generally, in condensed phase, data reproducibility requires the proper account of environmental effects. For instance, polarizable continuum models[34] can be employed to describe innocent solvents at a negligible additional cost with respect to the corresponding simulation in vacuo. Such a model can be improved by incorporating a reduced number of explicit solvent molecules in the treatment,[151] provided that they occupy well-defined positions and are quite strongly bonded to the solute. In this respect, topological models for the automatic definition of the number and position of strongly bonded solvent molecules are under active development[234] and the definition of widely accepted standards would be a very important achievement.

Finally, while the issue of a general standard addressed above (first level) is a basic need for collaborations, a mention to the information accompanying publications is deserved. This does not involve program outputs, the collection (in tables) of spectroscopic parameters being usually exhaustive. However, cartesian coordinates for the molecular systems investigated are generally provided, while more rarely the force constants **[G]** describing a portion of PES are reported.

[H1] 6. Limitations and optimisations

Since its very beginning, computational spectroscopy has focused on deriving spectroscopic parameters to support the analysis of experimental spectra. In fact, interpretation of experimental data is often a difficult task. This is due to the fact the observed spectroscopic behavior derives from the interplay of different effects, whose specific roles are difficult to disentangle. Furthermore, the theoretical model used for their interpretation might be oversimplified.

Pushing the treatment of the electronic and nuclear problems to the limit ensures rigorous analyses, quantitative results, and correct interpretations of the spectroscopic outcomes. However, such accurate approaches involve high computational costs and efforts and, therefore, they are restricted to small, isolated molecules (as briefly addressed in section 5). Increasing the size and complexity of the systems often requires a sacrifice of accuracy for interpretability, thus leading to qualitative descriptions. In such cases, the main limitation is an oversimplification that might lead to the right answer for the wrong reason, which means to obtain the correct reproduction of the spectral features based on wrong spectroscopic parameters. In turn, this might also mean the derivation of wrong physicochemical properties, or even incorrect interpretation on what molecular species are actually observed. The only way to mitigate this is to try to apply a physically sounded model and possibly take corrective actions based on similar (but smaller) systems already investigated. However, the selection of the fragments and the treatment of the boundary among them are open questions that require considerable experience, good knowledge of the system to be investigated and, above all, further algorithmic developments and implementations.

Modern computational spectroscopy aims to bridge the gap between sophisticated experimental techniques and oversimplified analyses, also exploiting visualization and simulation techniques. An interesting example is provided by oxirane derivatives, whose spectral features could not be described by more simplified theoretical models. State-of-the-art simulations of IR, Raman, VCD, ROA, OPA, ECD are in good agreement with their experimental counterparts allowing also to reconcile theory and experiment.[35,112,235,236]

As mentioned in the previous section and along this primer, accurate methodologies have been developed for the treatment of small- to medium-sized molecular systems (see e.g. refs. [34,150,237]), linear-scaling and hybrid approaches (that will be addressed later in this section) allowing for their extension to larger systems. However, a current challenge for computational spectroscopy tools is provided by large flexible molecules, for which the analysis of the conformational PES is the first obstacle to be overcome. In fact, in order to correctly interpret their spectroscopic features, the knowledge of the structures contributing to them is mandatory. In this respect, in the last decade, significant progress has been made thanks to stochastic (molecular dynamics or Monte Carlo) techniques[150] and machine-learning algorithms,[230,234] all of them helping in deriving an exhaustive account of the number and type of conformers relevant for the spectroscopic analysis.

Moving to spectral simulations, the number and types of LAMs are still a strong limitation for accuracy. In fact, while a decoupling (or a minimization of the coupling) between SAMs and LAMs together with a variational treatment of the latter modes can pose the basis for an accurate spectroscopic treatment, this approach is currently effective for dealing with only one LAM.[238] Nevertheless, a further issue is the level of theory employed for the description of the portion of PES (or PESs) required to the spectroscopic technique under consideration. In fact, the scaling of most of the accurate QC models is prohibitive, thus hampering their application already to medium-sized molecular systems. However, for the latter, composite schemes often provide an effective solution. For larger systems, a possible way-out is offered by fragment-based approaches such the molecules-in-molecules,[238] which is a multilevel partitioning approach coupled with electronic structure studies at different levels of theory with the final aim of providing a hierarchical strategy for systematically improving the computed results. At the same time, further improvements on the reliability of methods rooted in the density functional theory (e.g. double-hybrid functionals, long range corrections, etc.)[239] and the development of linear-scaling techniques, especially for the exact-exchange[240] and MP2[241] parts, paves the route toward more reliable computations for large systems. In parallel, explicitly-correlated F12 treatments[105] allows the reduction of the basis-set dimensions in electronic structure computations, thus improving the reachable accuracy. A further step is provided by local-correlation treatments based on PNO,[106,107] which - as already mentioned - allow for improving the scaling of coupled cluster treatments with the number of electrons.

While being aware that limitations and optimizations in the field of computational molecular spectroscopy cannot be exhaustively addressed in this section, it should be noted that the accurate spectroscopic characterization of open-shell species is more challenging than that of their closed-shell counterparts, regardless of the size of the molecular system under consideration.[242] The situation is even more involved for systems showing large static correlation effects (e.g. low-spin states of most transition metals, see section 4.3), with methods rooted in the DMRG[136] or quantum Monte Carlo[243] being good alternatives with respect to multi-reference methods and opening promising routes toward effective treatments.

[H1] 7. Outlook

The previous sections have shown that the ongoing developments of hardware and software are allowing the study of the spectroscopic outcomes of several systems and processes of current scientific and technological interest with an accuracy simply unthinkable even ten years ago. Furthermore, the range of applications of computational spectroscopy has considerably widened including now diverse fields as astrochemistry,[244] atmospheric chemistry[245] or catalysis,[220] just to mention a few. However, the historical dichotomy between accuracy and interpretability (not to speak of feasibility and user-friendliness)[34] remains one of the hardest obstacles against the definitive transformation of computational spectroscopy from a highly specialized field to a general-purpose tool aiding both theoretically- and experimentally-oriented scientists in their research work. This aspect is even more important since state-of-the-art spectroscopic investigations usually involve the contemporary use of several experimental techniques and new, highly sophisticated computational tools are constantly proposed and implemented. In this framework, the most needed developments concern the extension of accurate evaluations of spectroscopic parameters from small semi-rigid closed-shell systems containing light atoms in the gas phase[237] to a general workflow for the spectroscopic characterization of large, flexible chromophores in condensed phases.[246] While most of the building blocks of the procedure are already available, their integration into a robust, general, and user-friendly tool calls for further developments and validations.

One aspect to consider is the extension and validation of composite models for electronic structure calculations to transition metals and heavy atoms, large systems, open-shell species, and excited electronic states. Possible routes to achieve this include explicitly-correlated coupled-cluster approaches,[105,247] localized treatments of correlation (e.g. local pair natural orbitals, LPNO **[G]**),[231,232] effective treatment of static correlation,[136,248] further improvements of density functionals for comprehensive scans of PESs[249] as well as reliable structure and force-field evaluations,[239] more effective treatments of excited electronic states.[250,251]

Another important aspect to take into consideration is the vis-à-vis comparisons between computed and experimental spectra, including positions and heights (i.e. intensities) of band maxima, but also spectral shapes[61] and the extension of such comparisons to all possible spectroscopies. This in turn requires accurate yet effective evaluations of all the parameters needed by different spectroscopic techniques[133,252] and their post-processing. Indeed, the vis-à-vis comparison is probably the best way to exploit the interplay of experiment and theory.

To improve the spectroscopic analysis of flexible molecules, in particular in the fields of rotational and vibrational spectroscopies, general-purpose treatments of their spectra in terms of curvilinear internal coordinates, possibly coupling the variational treatment of LAMs with the perturbative treatment of SAMs and couplings, need to be developed and implemented.[249,253] A promising alternative is offered by integrated treatments of electronic and high-frequency nuclear motions by means of nuclear-electronic orbitals.[254] In the framework of electronic spectroscopies, the extension to large chromophores of anharmonic vibronic models[255] for absorption and emission electronic spectroscopy, also including chiroptical spectra, is important to take a step forward in the characterization of biomolecules.

Effective coupling between explicit dynamic treatment of soft degrees of freedom (e.g., torsions around single bonds, ring puckerings, and solvent fluctuations) involving large-mass moieties (for which classical equations of motion are fully adequate) and quantum-mechanical treatment of hard degrees of freedom.[256] These developments will allow the accurate yet effective treatment of large flexible systems in condensed phases, which is hardly feasible with current software and hardware.

Integration of the variational (QM, QM/QM' or QM/MM, MM standing for molecular mechanics and the "slash" used to denote that two levels of treatments are employed, thus implying a partitioning of the system) evaluation of large-scale deformations (e.g. different conformers and/or different topologies of solute-solvent interactions in the cybotactic region) with the perturbative (e.g. PMM **[G]**) evaluation of fluctuations within different basins.[151] Also in this case, clever coupling of variational (QM/QM, etc.) and perturbative (PMM) approaches will strongly reduce the computer requirements (both time and memory) without sacrificing the accuracy of the overall computation.

In the framework of ro-vibrational spectroscopy, effective determination of partition functions (and/or density and number of states) beyond the rigid-rotor/harmonic-oscillator model[257,258] would allow the computation of accurate thermodynamic functions and reaction rates for flexible systems possibly in condensed phases.

Implementation of artificial-intelligence tools for the sampling of PESs after their training with reference to state-of-the-art QC results paves the route toward very accurate energies, structures and force fields of both local minima and transition states at a cost comparable to that of inexpensive MM methods.[230] On the other hand, implementation of immersive virtual- and augmented-reality tools for the effective setup of general spectroscopic studies and the interactive analysis of the results[259] can revolutionize the whole field (as well as many others), thereby changing the perspective from abstraction to perception by bringing the objects under study to the same spatial-temporal scale of human beings. In a more distant perspective, effective use of quantum computing will improve the rate of state-of-the-art techniques.[260] As a matter of fact, the exact solution of the Schrödinger equation has an intrinsic exponential scaling with the dimension of the problem and the most accurate QC techniques scale as high powers (at least 10^8) of the number of active particles. In parallel, the speed of traditional computers scales linearly with the number of cores, whereas the scaling of quantum computers is, in principle, exponential.

In summary, in this Primer --focusing on a selection of molecular spectroscopic techniques-- we have shown how Computational Spectroscopy works, briefly presenting its foundations as well as significant results and applications. Furthermore, along this Primer, the fundamental role of Computational Spectroscopy in supporting and complementing experimental investigations has been addressed. A critical analysis of its current limitations and possible improvements has also been performed, which has been concluded by an exhaustive presentation of future perspectives and needs.

Glossary (terms in text annotated with [G])

AC	Absolute Configuration: indicates the spatial arrangement of atoms in a chiral system and its stereochemical description.
AILFT	Ab-initio ligand field theory: is a method connecting the results of ab initio calculations with the parameters entering ligand field theory.
Anharmonicity	Deviation from the harmonic-oscillator behavior.
BO (approximation)	The Born-Oppenheimer Approximation: is the assumption that the motion of atomic nuclei and electrons can be treated separately, based on the much larger mass of nuclei.
CASPT2	Complete active space perturbation theory to second order: is one specific generalization of MP2 (see below) to multiconfigurational reference wave-functions.
CC (theory)	Coupled-cluster (theory): is a hierarchy of electron correlation methods that, by means of an exponential Ansatz, systematically converge to the exact solution of the molecular Schrödinger equation starting from the independent particle Hartree-Fock model.
CD	Circular Dichroism: is dichroism (splitting of a beam of light into two beams with different wavelengths) involving circularly polarized light, i.e., the differential absorption of left- and right-handed light.
CCSD(T)	CC method that considers full account of single and double excitations and a perturbative treatment of triple excitations.
CFT	Crystal field theory: describes the splitting of the (relativistic) many particle multiplet states of an ion in a d^n or f^n configuration incurred by the electrostatic interaction with its coordinating ligands that are treated as point charges.
CIS	Configuration interaction (i.e. mixing of ground and excited electronic states) including only single excitations from a reference Slater determinant.
Combination band	A combination band is observed when two or more vibrations are excited simultaneously
Conformer	Isomer that can be converted into another one by rotation about a formally single bond.
Contact transformation	Unitary transformation with an exponential operator U = exp(*i*S), where S is Hermitean and antisymmetric with respect to time reversal, thus ensuring that U is unitary and invariant to time reversal.
Cybotactic (region)	The region around a solute molecule including solvent molecules belonging to the first solvation shell, i.e. showing close solute-solvent contacts
DFT	Density functional theory: is a quantum-mechanical method in which the properties of a many-electron system are determined using functionals (i.e. functions of another function) of the spatially dependent electron density and, possibly, its derivatives.
DMC	Diffusion Monte Carlo: provides a Monte Carlo based approach for obtaining the exact ground state solution to Equation 2.
DMRG	Density matrix renormalization group: is a very efficient numerical variational technique devised to obtain the lowest-energy wavefunction of a given Hamiltonian expressed in terms of a matrix product state.
(DL)PNO	(Domain-based local) pair natural orbitals: are electron pair specific localized natural orbitals expanded in a set of local atomic orbitals belonging to pair specific domains.
Double-perturbative approach	Simultaneous perturbative treatment of the energy and one property (e.g. the electric dipole moment in infrared spectroscopy) around a stationary point.
ECD	Electronic version of the circular dichroism (see above)
Electron correlation	Electron Correlation: describes the effects of electron-electron interactions beyond the mean field Hartree-Fock model.
Electron Correlation: Dynamic	Electron correlation effects describing the "instantaneous" electron-electron interaction if groups of electrons approach each other in close proximity.
Electron Correlation: Static	Electron correlation effects describing the correlated motion of electrons not captured correctly by the single Slater determinant treatment offered by the Hartree-Fock model.
Energy level	According to quantum mechanics (see below), the allowed energy for a system is not continuous, but discretized in energy levels.

Ensemble of walkers	A large number of virtual copies of a single particle moving randomly over a given potential energy surface.
EOM	Equation-of-Motion: in a quantum chemistry context it refers to the coupled cluster treatment of electronically excited or ionized states
ESR	Electron spin resonance: is a spectroscopic techniques equivalent to NMR (see below) but dealing with excitation of the electronic spins in open-shell systems.
EPR	Electron paramagnetic resonance: is a synonym of electron spin resonance.
Force constant	Derivative of the potential energy with respect to nuclear coordinates evaluated at the minimum structure (e.g. the quadratic force constant is the second derivative).
Fundamental band	Vibrational transition from the vibrational ground state to the first excited state of a given vibrational mode.
FWHM/HWHM	Full/Half width at half maximum: is the width (or half the width) between the two points where the value of the function is its half maximum.
Hamiltonian	In quantum mechanics, it is the operator corresponding to the energy of a system.
Harmonic	Model in which the vibrational motion is described in terms of masses attached to a spring, whose energy is governed by a quadratic potential.
Hybrid/Double-hybrid density functional	Families of density functionals including a percentage of Hartree-Fock exchange (hybrid) and MP2-type correlation (only double-hybrid).
Imaginary time	Since the time evolution of a quantum system starting from time t_0 is governed by exp[-i*H*(t-t0)] where *H* is the Hamiltonian operator, τ = *i*(t-t0) is usually referred to as imaginary time.
Infrared spectroscopy	Spectroscopy using the infrared region of the electromagnetic field to study the excitation of the vibrational states of molecules.
LFT	Ligand Field Theory: a semi-empirical “perturbed ion” model, based on CFT, that describes the electronic structure and properties of transition metal complexes.
Line-shape function	A mathematical function (usually Gaussian, Lorentzian or a combination of both) describing phenomenologically the shape of a spectral band.
MCD	The Circular Dichroism induced by a static, longitudinal external magnetic field.
LAM	Large amplitude motion: refers to a molecular vibration whose amplitude is so large that the harmonic oscillator model is no more a reliable zero-order approximation.
Mössbauer isomer shift	The shift in resonance frequency of the nuclear gamma-ray transition in a Mössbauer active isotope (e.g. ^{57}Fe) caused by its interaction with the molecular environment.
MM	Molecular mechanics (or force-field methods) uses classical type models to predict the energy of a molecule as a function of its conformation.
MP2	Møller-Plesset theory including many-body effects on top of the mean field Hartree-Fock reference wavefunction up to the second order of perturbation theory.
MRCI	Multi reference configuration interaction: extends the configuration interaction approach to multireference wavefunctions.
Multiplet	The ensemble of many particle states that arise from the distribution of a given number of electrons among sets of degenerate atomic or molecular orbitals under the action of the electron-electron (and perhaps the spin-orbit coupling) interaction.
NEVPT2	N-electron valence state perturbation theory to the second order: is a variant of second order multireference perturbation theory similar to CASPT2.
NMR	Nuclear magnetic resonance: is a spectroscopic technique based on the perturbation of nuclei in a strong constant magnetic field by a weak oscillating magnetic field (in their close environment), which produces an electromagnetic signal with a frequency related to the magnetic field at the nucleus.
Normal mode / Normal coordinate	Vibrational motion of the molecules where all atoms vibrate in phase with the same frequency but with different amplitudes, and the center of mass remains fixed. A normal coordinate is a linear combination of Cartesian displacement coordinates. The motion described by a normal coordinate is called a normal mode.
OPA	Spectroscopic technique in which one-photon absorption leads from the electronic ground state to an excited electronic state.
OPE	Spectroscopic technique in which one-photon emission leads from an excited electronic state to a less-excited (lower energy, usually the ground) state.

OR	Optical rotation: is the rotation angle of the polarization plane of polarized light issuing from its passage through a layer or a liquid and is determined by the concentration of chiral molecules and their structure in a substance.
Orbital splitting	Splitting of a specific orbital due to external factors (e.g. electric or magnetic field).
ORD	Optical rotatory dispersion: is the variation of the optical rotation of a substance with a change in the wavelength of light.
Overtone	Vibrational transition involving the excitation of two or more quanta of a given vibration mode (i.e. the quantum number describing the vibrational energy levels change varies by two o more)
PCM	Polarizable continuum model: description of bulk solvent effects in terms of a polarizable continuum in which the solute is fully embedded.
PES	Potential energy surface (multi-dimensional, hyper-surface): describes the variations of the electron energy of a system in terms of suitable nuclear coordinates.
PMM	Perturbed matrix method: describes solvent effects on a quantum center in terms of CIS, whose elements are the energies of the isolated solute perturbed by the electric field produced by the different configurations of the solvent issuing from a molecular dynamics simulation.
Position array	Array containing the coordinates of the position of a specific point in a multi-dimensional space.
PS	Property surface (multi-dimensional): describes the variations of a property as a function of suitable nuclear coordinates.
QC	Quantum chemistry (quantum chemical being the corresponding adjective): refers to the application of quantum mechanics to chemistry.
QM	Quantum mechanics (quantum mechanical being the corresponding adjective): is a fundamental theory of contemporary physics that provides a description of the properties of the matter at the atomic and subatomic level.
Raman spectroscopy	Rotational or vibrational spectroscopy that exploits the Raman effect (inelastic scattering).
Rigid-rotor harmonic-oscillator model	A reference model in which a molecular system as a whole is described in terms of a rigid rotating object and in terms of decoupled harmonic oscillators for its vibrational motion.
ROA	Raman optical activity: is a vibrational spectroscopy based on the differential Raman scattering of left and right circularly polarized light due to molecular chirality.
Rotational Spectroscopy	Spectroscopy using the microwave region of the electromagnetic field to study the excitation of the rotational states of molecules.
Rovibrational Spectroscopy	Spectroscopy dealing with rotational and vibrational states of molecules.
SAM	Small amplitude motion/mode: refers to a molecular vibration whose amplitude is small enough so that the harmonic oscillator is a reliable zero-order approximation.
Schrödinger equation	Equation associated to the Hamiltonian operator: its resolution provides the allowed energy levels (eigenvalues) and the corresponding wave functions (eigenfunctions).
Slater determinant	Representation of a many particle 'mean-field' wavefunction in terms of the antisymmetrized products of single-electron wavefunctions (molecular orbitals).
SOC	Spin orbit coupling: refers to the coupling between the spin and the orbital angular momenta.
Spectroscopic transition	The passage between two energy levels, i.e. from an initial to a final state, detected by a spectroscopic technique.
SQUID	Magnetometer based on superconducting loops used to measure very low magnetic fields.
STEOM	Similarity transformed equations of motion (see above).
TDA	Tamm Dancoff approximation: is, from a practical point of view, a synonym of CIS.
Template approach	A model in which the structure of a molecular system is refined with reference to suitable fragments, whose structures are accurately known.
VCD	Vibrational version of the circular dichroism.
VCI	Vibrational configuration interaction: exploits the configuration interaction model to treat vibrational motions.

Vibronic spectroscopy	Spectroscopy involving the simultaneous excitations of vibrational and electronic states of molecules.
VPT2	Vibrational perturbation theory to second order: exploits perturbation theory to the second order to treat the vibrational motions.
VSCF	Vibrational self-consistent field: exploits the self-consistent model to treat the vibrational motion.
Wave function	Mathematical description of the quantum state of an isolated quantum system resulting from the corresponding Schrödinger equation.
ZFS	Zero field splitting: describes the lifiting of the degeneracy of the 2S+1 magnetic sublevels of a spin multiplet with total spin S in the absence of a magnetic field, caused by the effects of SOC and electron-electron spin-spin interactions.
ZPE	Zero-point energy: is the lowest energy that a quantum system may have, which, contrary to the classical case, is nonzero due to the Heisenberg uncertainty principle.

Author contributions

Introduction (V.B., M.B., F.N., C.P.); Experimentation (V.B., M.B., J.R.C., A. B. M., F.N., C.P.); Results (M.M., C.P., V.B., M.B., A.B.M., R.D., J.R.C.); Applications (M.M., C.P., D.C.C., F.N.); Reproducibility and data deposition (S.A., V.B., M.B., A.M.B., C.P.); Limitations and optimizations (S.A., V.B., M.B., J.R.C., C.P.); Outlook (V.B.); Overview of the Primer (C.P.).

Competing interests

All authors declare no competing interests.

Selected key references

[1] Nafie, L. A. in *Vibrational Optical Activity: Principles and Applications* (John Wiley & Sons, Chicheston, United Kingdom, 2011).
Book that provides a comprehensive description of the underlying theory of the chiroptical spectroscopic methods VCD and ROA, and includes computational and experimental aspects as well as applications.

[18] Neese, F., Petrenko, T., Ganyushin, D. & Olbrich, G. Advanced aspects of ab initio theoretical optical spectroscopy of transition metal complexes: Multiplets, spin-orbit coupling and resonance Raman intensities. *Coord. Chem. Rev.* **251**, 288-327 (2007).
Review reporting a careful analysis of quantum-chemical approaches for the study of transition metal complexes.

[33] Neese, F. Quantum Chemistry and EPR Parameters. *eMagRes* **6**, 1-22 (2017).
The most recent and exhaustive review on the quantum-chemical computation of the parameters involved in the EPR spectroscopy.

[34] Puzzarini, C., Bloino, J., Tasinato, N. & Barone, V. Accuracy and Interpretability: The Devil and the Holy Grail. New Routes across Old Boundaries in Computational Spectroscopy. *Chem. Rev.* **119**, 8131-8191 (2019).
The most recent review on computational (rotational and vibrational) spectroscopy, also addressing the challenges of accuracy and interpretability.

[43] Franke, P. R., Stanton, J. F. & Douberly, G. E. How to VPT2: Accurate and Intuitive Simulations of CH Stretching Infrared Spectra Using VPT2+K with Large Effective Hamiltonian Resonance Treatments. *J. Phys. Chem. A* **125**, 1301-1324 (2021).
Recent instructive review on vibrational perturbation theory, also discussing in detail the treatment of resonances.

[61] Barone, V. The Virtual Multifrequency Spectrometer: a new paradigm for spectroscopy. *Wiley Interdiscip. Rev. Comput. Mol. Sci.* **6**, 86-110 (2016).
Recent review that introduces a new (also more intuitive) approach of computational spectroscopy based on the vis-à-vis comparison of calculated and experimental spectra instead of the mere computation of spectroscopic parameters.

[62] Bloino, J., Baiardi, A. & Biczysko, M. Aiming at an accurate prediction of vibrational and electronic spectra for medium-to-large molecules: An overview. *Int. J. Quantum Chem.* **116**, 1543-1574 (2016).
Tutorial review presenting detailed computational protocol and guidelines for the simulation of vibrational and vibrationally resolved electronic spectra for medium-to-large molecular systems of increasing flexibility.

[65] Srebro-Hooper, M. & Autschbach, J. Calculating Natural Optical Activity of Molecules from First Principles. *Annu. Rev. Phys. Chem.* **68**, 399-420 (2017).
Recent review that outlines computational models and methodological developments for chiroptical spectroscopic methods which include OR, ECD, VCD and ROA.

[84] Suhm, M. A. & Watts, R. O. Quantum Monte Carlo studies of vibrational states in molecules and clusters. *Phys. Rep.* **204**, 293-329 (1991).
Extensive review of the Diffusion Monte Carlo approach and its application to studies of nuclear quantum effects in molecules and clusters.

[85] Anderson, J. B. A random-walk simulation of the Schrödinger equation: H^{+3}. *J. Chem. Phys.* **63**, 1499-1503 (1975).
Key publication that introduced the diffusion Monte Carlo approaches described in this primer to the chemistry community.

[110] Grimme, S. Semiempirical hybrid density functional with perturbative second-order correlation. *J. Chem. Phys.* **124**, 034108 (2006).
Key publication reporting the introduction of double-hybrid functionals, which in turn allow quantitative spectroscopic studies by DFT.

[107] Neese, F., Wennmohs, F. & Hansen, A. Efficient and accurate local approximations to coupled-electron pair approaches: An attempt to revive the pair natural orbital method. *J. Chem. Phys.* **130**, 114108 (2009).
Key publication reporting the development and validation of an approach to extend the application of accurate quantum-chemical methods to large molecular systems.

[136] Baiardi, A. & Reiher, M. The density matrix renormalization group in chemistry and molecular physics: Recent developments and new challenges. *J. Chem. Phys.* **152**, 040903 (2020).
The most recent review on the use of methods rooted in the density matrix renormalization group for vibrational and electronic spectroscopy.

[140] Puzzarini, C., Stanton, J. F. & Gauss, J. Quantum-chemical calculation of spectroscopic parameters for rotational spectroscopy. *Int. Rev. Phys. Chem.* **29**, 273-367 (2010).
The most authoritative review on computational rotational spectroscopy.

[174]. Bogaerts, J. et al. A combined Raman optical activity and vibrational circular dichroism study on artemisinin-type products. *Phys. Chem. Chem. Phys.* **22**, 18014-18024 (2020).
A very recent study that demonstrates the combined use of two chiroptical spectroscopic methods, VCD and ROA, in determining the AC of a molecule with seven chiral centers.

[188] Puzzarini, C., Barone, V. A never-ending story in the sky: the secrets of chemical evolution, *Phys. Life Rev.* **32**, 59-94 (2020).
Recent review addressing the role of spectroscopic investigation for the characterization of molecules of astrochemical interest and their detection in space.

[200] Keutsch, F. N. & Saykally, R. J. Water clusters: Untangling the mysteries of the liquid, one molecule at a time. *Proc. Natl. Acad. Sci. U.S.A.* **98**, 10533-10540 (2001).
Comprehensive review on how theory is used to predict and interpret experimental measurements of spectra for water clusters.

[213] Beć, K. B. & Huck, C. W. Breakthrough Potential in Near-Infrared Spectroscopy: Spectra Simulation. A Review of Recent Developments. *Front. Chem.* **7**, 48 (2019).
Detailed review on the computational methods used for calculating the near-infrared spectra of larger polyatomic molecules.

[230] Dral, P. O. Quantum Chemistry in the Age of Machine Learning. *J. Phys. Chem. Lett.* **11**, 2336-2347 (2020).
A general introduction on the use of machine learning in quantum chemistry.

[250] Loos, P.-F., Scemama, A. & Jacquemin, D. The Quest for Highly Accurate Excitation Energies: A Computational Perspective. *J. Phys. Chem. Lett.* **11**, 2374-2383 (2020).
Recent perspective article on accurate computations of excitation energies.

References

1 Nafie, L. A. in *Vibrational Optical Activity: Principles and Applications* (John Wiley & Sons, Chicheston, United Kingdom, 2011).

2 Merkt, F. & Quack, M. *Handbook of High-resolution Spectroscopy*. (John Wiley & Sons, New York, NY, YSA, 2011).

3 Laane, J. *Frontiers of Molecular Spectroscopy*. (Elsevier, Amsterdam, The Netherlands, 2008).

4 Berova, N., Nakanishi, K. & Woody, R. W. *Circular Dichroism: Principles and Applications*. 2 edn, (Wiley-VCH, New York, NY, USA, 2000).

5 Rijs, A. M. & Oomens, J. *Gas-phase IR Spectroscopy and Structure of Biological Molecules. Topics in Current Chemistry.* . Vol. 364 (Springer International Publishing, Switzerland, 2015).

6 Pulay, P., Meyer, W. & Boggs, J. E. Cubic force constants and equilibrium geometry of methane from Hartree–Fock and correlated wavefunctions. *J. Chem. Phys.* **68**, 5077-5085 (1978).

7 Obenchain, D. A. *et al.* Unveiling the Sulfur-Sulfur Bridge: Accurate Structural and Energetic Characterization of a Homochalcogen Intermolecular Bond. *Angew. Chem. Int. Ed.* **57**, 15822-15826 (2018).

8 Caminati, W. in *Handbook of High-resolution Spectroscopy* (eds F. Merkt & M. Quack) (John Wiley & Sons, New York, NY, YSA, 2011).

9 Park, G. B. & Field, R. W. Perspective: The first ten years of broadband chirped pulse Fourier transform microwave spectroscopy. *J. Chem. Phys.* **144**, 200901 (2016).

10 Xie, F. *et al.* Discovering the Elusive Global Minimum in a Ternary Chiral Cluster: Rotational Spectra of Propylene Oxide Trimer. *Angew. Chem. Int. Ed.* **59**, 22427-22430 (2020).

11 Wang, J. *et al.* The Unexplored World of Cycloalkene–Water Complexes: Primary and Assisting Interactions Unraveled by Experimental and Computational Spectroscopy. *Angew. Chem. Int. Ed.* **58**, 13935 –13941 (2019).

12 Alonso, J. L. & López, J. C. in *Gas-Phase IR Spectroscopy and Structure of Biological Molecules* (eds Anouk M. Rijs & Jos Oomens) 335-401 (Springer International Publishing, 2015).

13 Atanasov, M. *et al.* First principles approach to the electronic structure, magnetic anisotropy and spin relaxation in mononuclear 3d-transition metal single molecule magnets. *Coord. Chem. Rev.* **289-290**, 177-214 (2015).

14 Barone, V. in *Computational strategies for spectroscopy: from small molecules to nano systems* (John Wiley & Sons, Hoboken, New Jersey, 2011).

15 Grunenberg, J. in *Computational spectroscopy: methods, experiments and applications* (John Wiley & Sons, Weinheim, Germany, 2011).

16 Jensen, P., Bunker P. R. . in *Computational Molecular Spectroscopy* (Wiley & Sons, Chichester, United Kingdom, 2000).

17 Neese, F. Prediction of molecular properties and molecular spectroscopy with density functional theory: From fundamental theory to exchange-coupling. *Coord. Chem. Rev.* **253**, 526-563 (2009).

18 Neese, F., Petrenko, T., Ganyushin, D. & Olbrich, G. Advanced aspects of ab initio theoretical optical spectroscopy of transition metal complexes: Multiplets, spin-orbit coupling and resonance Raman intensities. *Coord. Chem. Rev.* **251**, 288-327 (2007).

19 Mata, R. A. & Suhm, M. A. Benchmarking Quantum Chemical Methods: Are We Heading in the Right Direction? *Angew. Chem. Int. Ed.* **56**, 11011-11018 (2017).

20 Born, M. & Oppenheimer, R. Zur quantentheorie der molekeln. *Ann. Phys. (Berlin)* **389**, 457-484 (1927).

21 Eckart, C. Some Studies Concerning Rotating Axes and Polyatomic Molecules. *Phys. Rev.* **47**, 552-558 (1935).
22 Sayvetz, A. The Kinetic Energy of Polyatomic Molecules. *J. Chem. Phys.* **7**, 383-389 (1939).
23 Watson, J. K. G. Simplification of the molecular vibration-rotation hamiltonian. *Mol. Phys.* **15**, 479-490 (1968).
24 Watson, J. K. G. The vibration-rotation hamiltonian of linear molecules. *Mol. Phys.* **19**, 465-487 (1970).
25 Furtenbacher, T., Császár, A. G. & Tennyson, J. MARVEL: measured active rotational–vibrational energy levels. *J. Mol. Spectrosc.* **245**, 115-125 (2007).
26 Furtenbacher, T. & Császár, A. G. On employing $H_2{}^{16}O$, $H_2{}^{17}O$, $H_2{}^{18}O$, and $D_2{}^{16}O$ lines as frequency standards in the 15–170 cm^{-1} window. *J. Quant. Spectrosc. Radiat. Transfer* **109**, 1234-1251 (2008).
27 Aliev, M. R. & Watson, J. K. G. in *Molecular Spectroscopy: Modern Research* (ed Narahari Rao K.) Ch. Higher-order effects in the vibration-rotation spectra of semirigid molecules 1-67 (Academic Press, London, 1985).
28 Gordy, W. & Cook, R. L. in *Microwave Molecular Spectra* (ed Weissberger A) (Wiley, New York, 1984).
29 Watson, J. K. G. in *Vibrational Spectra and Structure: a series of advances* (ed Durig J. R.) (Elsevier, Amsterdam, 1977).
30 Kaupp, M., Buhl, M. & Malkin, V. G. in *Calculation of NMR and EPR Parameters. Theory and Applications* (eds Kaupp M., Buhl M., & Malkin V. G.) (Wiley, Weinheim, 2004).
31 Barone, V. & Polimeno, A. in *Electron Paramagnetic Resonance: A Practitioner's Toolkit* (eds Brustolon M. & Giamello E.) Ch. The Virtual Electron Paramagnetic Resonance Laboratory: A User Guide to ab initio Modeling, 251-284 (John Wiley & Sons, Hoboken, New Jersey, 2008).
32 Jose, K. V. & Raghavachari, K. Fragment-Based Approach for the Evaluation of NMR Chemical Shifts for Large Biomolecules Incorporating the Effects of the Solvent Environment. *J. Chem. Theory Comput.* **13**, 1147-1158 (2017).
33 Neese, F. Quantum Chemistry and EPR Parameters. *eMagRes* **6**, 1-22 (2017).
34 Puzzarini, C., Bloino, J., Tasinato, N. & Barone, V. Accuracy and Interpretability: The Devil and the Holy Grail. New Routes across Old Boundaries in Computational Spectroscopy. *Chem. Rev.* **119**, 8131-8191 (2019).
35 Bloino, J., Biczysko, M. & Barone, V. Anharmonic Effects on Vibrational Spectra Intensities: Infrared, Raman, Vibrational Circular Dichroism, and Raman Optical Activity. *J. Phys. Chem. A* **119**, 11862-11874 (2015).
36 Nielsen, H. H. The Vibration-Rotation Energies of Molecules. *Rev. Mod. Phys.* **23**, 90-136 (1951).
37 Mills, I. A. in *Molecular Spectroscopy: Modern Research* (eds K. Narahari Rao & C. Weldon Mathews) (Academic Press, New York, NY, USA, 1972).
38 Barone, V. Anharmonic vibrational properties by a fully automated second-order perturbative approach. *J. Chem. Phys.* **122**, 14108 (2005).
39 Bloino, J. & Barone, V. A second-order perturbation theory route to vibrational averages and transition properties of molecules: General formulation and application to infrared and vibrational circular dichroism spectroscopies. *J. Chem. Phys.* **136**, 124108 (2012).
40 Vázquez, J. & Stanton, J. F. Simple(r) algebraic equation for transition moments of fundamental transitions in vibrational second-order perturbation theory. *Mol. Phys.* **104**, 377-388 (2006).
41 Willetts, A., Handy, N. C., Green, W. H. & Jayatilaka, D. Anharmonic corrections to vibrational transition intensities. *J. Phys. Chem.* **94**, 5608-5616 (1990).
42 Császár, A. G. Anharmonic molecular force fields. *WIREs Comput. Mol. Sci.* **2**, 273-289 (2012).

43 Franke, P. R., Stanton, J. F. & Douberly, G. E. How to VPT2: Accurate and Intuitive Simulations of CH Stretching Infrared Spectra Using VPT2+K with Large Effective Hamiltonian Resonance Treatments. *J. Phys. Chem. A* **125**, 1301-1324 (2021).

44 Cornaton, Y., Ringholm, M., Louant, O. & Ruud, K. Analytic calculations of anharmonic infrared and Raman vibrational spectra. *Phys. Chem. Chem. Phys.* **18**, 4201-4215 (2016).

45 Maslen, P. E., Jayatilaka, D., Colwell, S. M., Amos, R. D. & Handy, N. C. Higher analytic derivatives. II. The fourth derivative of self-consistent-field energy. *J. Chem. Phys.* **95**, 7409-7417 (1991).

46 Piccardo, M., Bloino, J. & Barone, V. Generalized vibrational perturbation theory for rotovibrational energies of linear, symmetric and asymmetric tops: Theory, approximations, and automated approaches to deal with medium-to-large molecular systems. *Int. J. Quantum Chem.* **115**, 948-982 (2015).

47 Roy, T. K. & Gerber, R. B. Vibrational self-consistent field calculations for spectroscopy of biological molecules: new algorithmic developments and applications. *Phys. Chem. Chem. Phys.* **15**, 9468-9492 (2013).

48 Neff, M. & Rauhut, G. Toward large scale vibrational configuration interaction calculations. *J. Chem. Phys.* **131**, 124129 (2009).

49 Christiansen, O. Vibrational coupled cluster theory. *J. Chem. Phys.* **120**, 2149-2159 (2004).

50 Erfort, S., Tschöpe, M. & Rauhut, G. Toward a fully automated calculation of rovibrational infrared intensities for semi-rigid polyatomic molecules. *J. Chem. Phys.* **152**, 244104 (2020).

51 Biczysko, M., Bloino, J., Santoro, F. and Barone, V. in *Computational Strategies for Spectroscopy: From Small Molecules to Nano Systems* (ed Barone V) Ch. Time-Independent Approaches to Simulate Electronic Spectra Lineshapes: From Small Molecules to Macrosystems, 361-443 (John Wiley & Sons, Hoboken, New Jersey, 2011).

52 Bloino, J., Biczysko, M., Santoro, F. & Barone, V. General Approach to Compute Vibrationally Resolved One-Photon Electronic Spectra. *J. Chem. Theoy Comput.* **6**, 1256-1274 (2010).

53 Baiardi, A., Bloino, J. & Barone, V. General Time Dependent Approach to Vibronic Spectroscopy Including Franck–Condon, Herzberg–Teller, and Duschinsky Effects. *J. Chem. Theoy Comput.* **9**, 4097-4115 (2013).

54 Franck, J. & Dymond, E. G. Elementary processes of photochemical reactions. *Trans. Faraday Society* **21**, 536-542 (1926).

55 Condon, E. U. Nuclear Motions Associated with Electron Transitions in Diatomic Molecules. *Phys. Rev.* **32**, 858-872 (1928).

56 Herzberg, G. & Teller, E. Schwingungsstruktur der Elektronenübergänge bei mehratomigen Molekülen. *Z. Phys. Chem.* **21B**, 410 - 446 (1933).

57 Duschinsky, F. *Acta Physicochim. URSS.* 551 (1937).

58 Baiardi, A., Bloino, J. & Barone, V. General formulation of vibronic spectroscopy in internal coordinates. *J. Chem. Phys.* **144**, 084114 (2016).

59 Reimers, J. R. A practical method for the use of curvilinear coordinates in calculations of normal-mode-projected displacements and Duschinsky rotation matrices for large molecules. *J. Chem. Phys.* **115**, 9103-9109 (2001).

60 Baiardi, A., Bloino, J. & Barone, V. Simulation of Vibronic Spectra of Flexible Systems: Hybrid DVR-Harmonic Approaches. *J. Chem. Theoy Comput.* **13**, 2804-2822 (2017).

61 Barone, V. The Virtual Multifrequency Spectrometer: a new paradigm for spectroscopy. *Wiley Interdiscip. Rev. Comput. Mol. Sci.* **6**, 86-110 (2016).

62 Bloino, J., Baiardi, A. & Biczysko, M. Aiming at an accurate prediction of vibrational and electronic spectra for medium-to-large molecules: An overview. *Int. J. Quantum Chem.* **116**, 1543-1574 (2016).

63 Autschbach, J. in *Comprehensive Chiroptical Spectroscopy: Instrumentation, Methodologies, and Theoretical Simulations, Volume 1* (eds Berova N, Polavarapu P L, Nakanishi K, &

Woody R W) Ch. AB Initio Electronic Circular Dichroism and Optical Rotatory Dispersion: From Organic Molecules to Transition Metal Complexes, 593-642 (John Wiley & Sons, Hoboken, New Jersey, 2011).

64 Crawford, T. D. in *Comprehensive Chiroptical Spectroscopy: Instrumentation, Methodologies, and Theoretical Simulations, Volume 1* (eds Berova N, Polavarapu P L, Nakanishi K, & Woody R W) Ch. High-Accuracy Quantum Chemistry and Chiroptical Properties, 675-697 (John Wiley & Sons, Hoboken, New Jersey, 2011).

65 Srebro-Hooper, M. & Autschbach, J. Calculating Natural Optical Activity of Molecules from First Principles. *Annu. Rev. Phys. Chem.* **68**, 399-420 (2017).

66 Stephens, P. J., Devlin, F. J. & Cheeseman, J. R. in *VCD Spectroscopy for Organic Chemists* (CRC Press, Taylor & Francis Group, Boca Raton, Florida, 2012).

67 Ruud, K. in *Comprehensive Chiroptical Spectroscopy: Instrumentation, Methodologies, and Theoretical Simulations, Volume 1* (eds Berova N, Polavarapu P L, Nakanishi K, & Woody R W) Ch. AB Initio Methods for Vibrational Circular Dichroism and Raman Optical Activity, 699-727 (John Wiley & Sons, Hoboken, New Jersey, 2011).

68 Beer. Bestimmung der Absorption des rothen Lichts in farbigen Flüssigkeiten. *Ann. Phys. (Berlin)* **162**, 78-88 (1852).

69 Polavarapu, P. L. in *Chiroptical spectroscopy: fundamentals and applications* (CRC Press, Taylor & Francis Group, Boca Raton, Florida, 2016).

70 Stephens, P. J. & Harada, N. ECD cotton effect approximated by the Gaussian curve and other methods. *Chirality* **22**, 229-233 (2010).

71 Cheeseman, J. R. & Frisch, M. J. Basis Set Dependence of Vibrational Raman and Raman Optical Activity Intensities. *J. Chem. Theoy Comput.* **7**, 3323-3334 (2011).

72 Liégeois, V., Ruud, K. & Champagne, B. An analytical derivative procedure for the calculation of vibrational Raman optical activity spectra. *J. Chem. Phys.* **127**, 204105 (2007).

73 Nafie, L. A. Theory of Raman scattering and Raman optical activity: near resonance theory and levels of approximation. *Theor. Chem. Acc.* **119**, 39-55 (2008).

74 Barron, L. D. in *Molecular Light Scattering and Optical Activity* (Cambridge University Press, Cambridge, 2004).

75 Long, D. A. in *The Raman effect: a unified treatment of the theory of Raman scattering by molecules* (John Wiley & Sons, Chichester, United Kingdom, 2002).

76 Neugebauer, J., Reiher, M., Kind, C. & Hess, B. A. Quantum chemical calculation of vibrational spectra of large molecules--Raman and IR spectra for Buckminsterfullerene. *J. Comput. Chem.* **23**, 895-910 (2002).

77 Dzugan, L. C., DiRisio, R. J., Madison, L. R. & McCoy, A. B. Spectral signatures of proton delocalization in $H^+(H_2O)_{n=1-4}$ ions. *Faraday Discuss.* **212**, 443-466 (2018).

78 Tanaka, S., Roy, P.-N. & Mitas, L. in *Recent progress in Quantum Monte Carlo* Vol. 1234 (ACS Publications, Washington DC, 2016).

79 Tanaka, S., Rothstein, S. M. & Lester Jr, W. A. in *Advances in Quantum Monte Carlo* Vol. 1094 (ACS Publications, Washington DC, 2012).

80 Anderson, J. B. & Rothstein, S. M. in *Advances in Quantum Monte Carlo* Vol. 953 (ACS Publications, Washington DC, 2007).

81 Lester, W. A., Rothstein, S. M. & Tanaka, S. in *Recent Advances in Quantum Monte Carlo Methods: Part II Recent Advances in Computational Chemistry: Volume 2* (World Scientific, Singapore, 2002).

82 Lester, W. A., Rothstein, S. M. & Tanaka, S. in *Recent Advances in Quantum Monte Carlo Methods Recent Advances in Computational Chemistry* (World Scientific, Singapore, 1997).

83 McCoy, A. B. Diffusion Monte Carlo approaches for investigating the structure and vibrational spectra of fluxional systems. *Int. Rev. Phys. Chem.* **25**, 77-107 (2006).

84 Suhm, M. A. & Watts, R. O. Quantum Monte Carlo studies of vibrational states in molecules and clusters. *Phys, Rep.* **204**, 293-329 (1991).

85 Anderson, J. B. A random-walk simulation of the Schrödinger equation: H^{+3}. *J. Chem. Phys.* **63**, 1499-1503 (1975).
86 Anderson, J. B. Quantum chemistry by random walk. H ^2P, H^{+3} D_{3h} $^1A'_1$, H_2 $^3\Sigma^{+u}$, H_4 $^1\Sigma^{+g}$, Be ^1S. *J. Chem. Phys.* **65**, 4121-4127 (1976).
87 Barnett, R. N., Reynolds, P. J. & Lester, W. A. Monte Carlo algorithms for expectation values of coordinate operators. *J. Comput. Phys.* **96**, 258-276 (1991).
88 Petit, A. S., Wellen, B. A. & Mccoy, A. B. Using fixed-node diffusion Monte Carlo to investigate the effects of rotation-vibration coupling in highly fluxional asymmetric top molecules: Application to H_2D^+. *J. Chem. Phys.* **138** (2013).
89 Lee, H.-S., Herbert, J. M. & McCoy, A. B. Adiabatic diffusion Monte Carlo approaches for studies of ground and excited state properties of van der Waals complexes. *J. Chem. Phys.* **110**, 5481-5484 (1999).
90 Csaszar, A. G., Allen, W. D. & Schaefer III, H. F. In pursuit of the ab initio limit for conformational energy prototypes. *J. Chem. Phys.* **108**, 9751-9764 (1998).
91 Montgomery, J. A., Frisch, M. J., Ochterski, J. W. & Petersson, G. A. A complete basis set model chemistry. VI. Use of density functional geometries and frequencies. *J. Chem. Phys.* **110**, 2822-2827 (1999).
92 Demaison, J., Margules, L. & Boggs, J. E. The equilibrium C-Cl, C-Br, and C-I bond lengths from ab initio calculations, microwave and infrared spectroscopies, and empirical correlations. *Struct. Chem.* **14**, 159-174 (2003).
93 Puzzarini, C. Extrapolation to the Complete Basis Set Limit of Structural Parameters: Comparison of Different Approaches. *J. Phys. Chem. A* **113**, 14530-14535 (2009).
94 Puzzarini, C. & Barone, V. Extending the molecular size in accurate quantum-chemical calculations: the equilibrium structure and spectroscopic properties of uracil. *Phys. Chem. Chem. Phys.* **13**, 7189-7197 (2011).
95 Alessandrini, S., Barone, V. & Puzzarini, C. Extension of the "Cheap" Composite Approach to Noncovalent Interactions: The jun-ChS Scheme. *J. Chem. Theory Comput.* **16**, 988-1006 (2020).
96 Tajti, A. *et al.* HEAT: High accuracy extrapolated ab initio thermochemistry. *J. Chem. Phys.* **121**, 11599-11613 (2004).
97 Heckert, M., Kállay, M., Tew, D. P., Klopper, W. & Gauss, J. Basis-set extrapolation techniques for the accurate calculation of molecular equilibrium geometries using coupled-cluster theory. *J. Chem. Phys.* **125**, 044108 (2006).
98 Puzzarini, C., Heckert, M. & Gauss, J. The accuracy of rotational constants predicted by high-level quantum-chemical calculations. I. Molecules containing first-row atoms. *J. Chem. Phys.* **128**, 194108 (2008).
99 Yu, Q. *et al.* Structure, Anharmonic Vibrational Frequencies, and Intensities of $NNHNN^+$. *J. Phys. Chem. A* **119**, 11623-11631 (2015).
100 Boese, A. D. *et al.* W3 theory: Robust computational thermochemistry in the kJ/mol accuracy range. *J. Chem. Phys.* **120**, 4129-4141 (2004).
101 Karton, A., Rabinovich, E., Martin, J. M. L. & Ruscic, B. W4 theory for computational thermochemistry: In pursuit of confident sub-kJ/mol predictions. *J. Chem. Phys.* **125**, 144108 (2006).
102 Peterson, K. A., Feller, D. & Dixon, D. A. Chemical accuracy in ab initio thermochemistry and spectroscopy: current strategies and future challenges. *Theor. Chem. Acc.* **131**, 1079 (2012).
103 Shavitt, I. & Bartlett, R. J. in *Many-Body Methods in Chemistry and Physics: MBPT and Coupled-Cluster Theory Cambridge Molecular Science* (Cambridge University Press, Cambridge, 2009).
104 Raghavachari, K., Trucks, G. W., Pople, J. A. & Head-Gordon, M. A fifth-order perturbation comparison of electron correlation theories *Chem. Phys. Lett.* **589**, 37-40 (2013).

105 Kong, L., Bischoff, F. A. & Valeev, E. F. Explicitly Correlated R12/F12 Methods for Electronic Structure. *Chem. Rev.* **112**, 75-107 (2012).

106 Neese, F., Hansen, A. & Liakos, D. G. Efficient and accurate approximations to the local coupled cluster singles doubles method using a truncated pair natural orbital basis. *J. Chem. Phys.* **131**, 064103 (2009).

107 Neese, F., Wennmohs, F. & Hansen, A. Efficient and accurate local approximations to coupled-electron pair approaches: An attempt to revive the pair natural orbital method. *J. Chem. Phys.* **130**, 114108 (2009).

108 Becke, A. D. Density-functional thermochemistry. III. The role of exact exchange. *J. Chem. Phys.* **98**, 5648-5652 (1993).

109 Lee, C., Yang, W. & Parr, R. G. Development of the Colle-Salvetti correlation-energy formula into a functional of the electron density. *Phys. Rev. B* **37**, 785-789 (1988).

110 Grimme, S. Semiempirical hybrid density functional with perturbative second-order correlation. *J. Chem. Phys.* **124**, 034108 (2006).

111 Møller, C. & Plesset, M. S. Note on an Approximation Treatment for Many-Electron Systems. *Phys. Rev.* **46**, 618-622 (1934).

112 Barone, V., Biczysko, M., Bloino, J. & Puzzarini, C. Accurate molecular structures and infrared spectra of trans-2,3-dideuterooxirane, methyloxirane, and trans-2,3-dimethyloxirane. *J. Chem. Phys.* **141**, 034107 (2014).

113 Barone, V., Biczysko, M., Bloino, J. & Puzzarini, C. Accurate structure, thermodynamic and spectroscopic parameters from CC and CC/DFT schemes: the challenge of the conformational equilibrium in glycine. *Phys. Chem. Chem. Phys.* **15**, 10094-10111 (2013).

114 Jurečka, P., Šponer, J., Černý, J. & Hobza, P. Benchmark database of accurate (MP2 and CCSD(T) complete basis set limit) interaction energies of small model complexes, DNA base pairs, and amino acid pairs. *Phys. Chem. Chem. Phys.* **8**, 1985-1993 (2006).

115 Řezáč, J., Riley, K. E. & Hobza, P. S66: A Well-balanced Database of Benchmark Interaction Energies Relevant to Biomolecular Structures. *J. Chem. Theoy Comput.* **7**, 2427-2438 (2011).

116 Řezáč, J., Bím, D., Gutten, O. & Rulíšek, L. Toward Accurate Conformational Energies of Smaller Peptides and Medium-Sized Macrocycles: MPCONF196 Benchmark Energy Data Set. *J. Chem. Theoy Comput.* **14**, 1254-1266 (2018).

117 Goerigk, L. *et al.* A look at the density functional theory zoo with the advanced GMTKN55 database for general main group thermochemistry, kinetics and noncovalent interactions. *Phys. Chem. Chem. Phys.* **19**, 32184-32215 (2017).

118 Biczysko, M., Panek, P., Scalmani, G., Bloino, J. & Barone, V. Harmonic and Anharmonic Vibrational Frequency Calculations with the Double-Hybrid B2PLYP Method: Analytic Second Derivatives and Benchmark Studies. *J. Chem. Theory Comput.* **6**, 2115-2125 (2010).

119 Barone, V., Biczysko, M. & Bloino, J. Fully anharmonic IR and Raman spectra of medium-size molecular systems: accuracy and interpretation. *Phys. Chem. Chem. Phys.* **16**, 1759-1787 (2014).

120 Shu, C., Jiang, Z. & Biczysko, M. Toward accurate prediction of amino acid derivatives structure and energetics from DFT: glycine conformers and their interconversions. *J. Mol. Model.* **26**, 129 (2020).

121 Brémond, É. *et al.* Benchmarking Density Functionals on Structural Parameters of Small-/Medium-Sized Organic Molecules. *J. Chem. Theoy Comput.* **12**, 459-465 (2016).

122 Risthaus, T., Steinmetz, M. & Grimme, S. Implementation of nuclear gradients of range-separated hybrid density functionals and benchmarking on rotational constants for organic molecules. *J. Comput. Chem.* **35**, 1509-1516 (2014).

123 Su, N. Q. & Xu, X. Beyond energies: geometry predictions with the XYG3 type of doubly hybrid density functionals. *Chem. Commun.* **52**, 13840-13860 (2016).

124 Witte, J., Goldey, M., Neaton, J. B. & Head-Gordon, M. Beyond Energies: Geometries of Nonbonded Molecular Complexes as Metrics for Assessing Electronic Structure Approaches. *J. Chem. Theoy Comput.* **11**, 1481-1492 (2015).

125 Yu, H. S., He, X., Li, S. L. & Truhlar, D. G. MN15: A Kohn–Sham global-hybrid exchange–correlation density functional with broad accuracy for multi-reference and single-reference systems and noncovalent interactions. *Chem. Sci.* **7**, 5032-5051 (2016).

126 Boussessi, R., Ceselin, G., Tasinato, N. & Barone, V. DFT meets the segmented polarization consistent basis sets: Performances in the computation of molecular structures, rotational and vibrational spectroscopic properties. *J. Mol. Struct.* **1208**, 127886 (2020).

127 Hanson-Heine, M. W. D. Benchmarking DFT-D Dispersion Corrections for Anharmonic Vibrational Frequencies and Harmonic Scaling Factors. *J. Phys. Chem. A* **123**, 9800-9808 (2019).

128 Loos, P.-F., Lipparini, F., Boggio-Pasqua, M., Scemama, A. & Jacquemin, D. A Mountaineering Strategy to Excited States: Highly Accurate Energies and Benchmarks for Medium Sized Molecules. *J. Chem. Theoy Comput.* **16**, 1711-1741 (2020).

129 Brémond, E., Savarese, M., Adamo, C. & Jacquemin, D. Accuracy of TD-DFT Geometries: A Fresh Look. *J. Chem. Theoy Comput.* **14**, 3715-3727 (2018).

130 Egidi, F. *et al.* Effective Inclusion of Mechanical and Electrical Anharmonicity in Excited Electronic States: VPT2-TDDFT Route. *J. Chem. Theoy Comput.* **13**, 2789-2803 (2017).

131 Bomble, Y. J. *et al.* Equation-of-motion coupled-cluster methods for ionized states with an approximate treatment of triple excitations. *J. Chem. Phys.* **122**, 154107 (2005).

132 Roos, B. O., Lindh, R., Malmqvist, P. Å., Veryazov, V. & Widmark, P.-O. in *Multiconfigurational Quantum Chemistry* (John Wiley & Sons, Hoboken, New Jersey, 2016).

133 Auer, A. A. *et al.* A case study of density functional theory and domain-based local pair natural orbital coupled cluster for vibrational effects on EPR hyperfine coupling constants: vibrational perturbation theory versus ab initio molecular dynamics. *Mol. Phys.*, e1797916 (2020).

134 Datta, D., Saitow, M., Sandhöfer, B. & Neese, F. ^{57}Fe Mössbauer parameters from domain based local pair-natural orbital coupled-cluster theory. *J. Chem. Phys.* **153**, 204101 (2020).

135 Sirohiwal, A., Berraud-Pache, R., Neese, F., Izsák, R. & Pantazis, D. A. Accurate Computation of the Absorption Spectrum of Chlorophyll a with Pair Natural Orbital Coupled Cluster Methods. *J. Phys. Chem. B* **124**, 8761-8771 (2020).

136 Baiardi, A. & Reiher, M. The density matrix renormalization group in chemistry and molecular physics: Recent developments and new challenges. *J. Chem. Phys.* **152**, 040903 (2020).

137 Andersson, K., Malmqvist, P. Å. & Roos, B. O. Second-order perturbation theory with a complete active space self-consistent field reference function. *J. Chem. Phys.* **96**, 1218-1226 (1992).

138 Andersson, K., Malmqvist, P. A., Roos, B. O., Sadlej, A. J. & Wolinski, K. Second-order perturbation theory with a CASSCF reference function. *J. Phys. Chem.* **94**, 5483-5488 (1990).

139 Angeli, C., Cimiraglia, R., Evangelisti, S., Leininger, T. & Malrieu, J.-P. Introduction of n-electron valence states for multireference perturbation theory. *J. Chem. Phys.* **114**, 10252-10264 (2001).

140 Puzzarini, C., Stanton, J. F. & Gauss, J. Quantum-chemical calculation of spectroscopic parameters for rotational spectroscopy. *Int. Rev. Phys. Chem.* **29**, 273-367 (2010).

141 Licari, D., Tasinato, N., Spada, L., Puzzarini, C. & Barone, V. VMS-ROT: A New Module of the Virtual Multifrequency Spectrometer for Simulation, Interpretation, and Fitting of Rotational Spectra. *J. Chem. Theoy Comput.* **13**, 4382-4396 (2017).

142 Lesarri, A., Mata, S., López, J. C. & Alonso, J. L. A laser-ablation molecular-beam Fourier-transform microwave spectrometer: The rotational spectrum of organic solids. *Rev. Sci. Instrum.* **74**, 4799-4804 (2003).

143 Mancini, G., Fusè, M., Lazzari, F., Chandramouli, B. & Barone, V. Unsupervised search of low-lying conformers with spectroscopic accuracy: A two-step algorithm rooted into the island model evolutionary algorithm. *J. Chem. Phys.* **153**, 124110 (2020).

144 Császár, A. G. *et al.* The fourth age of quantum chemistry: molecules in motion. *Phys. Chem. Chem. Phys.* **14**, 1085-1106 (2012).

145 Baiardi, A., Stein, C. J., Barone, V. & Reiher, M. Vibrational Density Matrix Renormalization Group. *J. Chem. Theoy Comput.* **13**, 3764-3777 (2017).

146 Carter, S., Sharma, A. R., Bowman, J. M., Rosmus, P. & Tarroni, R. Calculations of rovibrational energies and dipole transition intensities for polyatomic molecules using MULTIMODE. *J. Chem. Phys.* **131**, 224106 (2009).

147 Begušić, T. & Vaníček, J. On-the-fly ab initio semiclassical evaluation of vibronic spectra at finite temperature. *J. Chem. Phys.* **153**, 024105 (2020).

148 Hirshberg, B., Sagiv, L. & Gerber, R. B. Approximate Quantum Dynamics using Ab Initio Classical Separable Potentials: Spectroscopic Applications. *J. Chem. Theoy Comput.* **13**, 982-991 (2017).

149 Gaigeot, M.-P. Theoretical spectroscopy of floppy peptides at room temperature. A DFTMD perspective: gas and aqueous phase. *Phys. Chem. Chem. Phys.* **12**, 3336-3359 (2010).

150 Pracht, P., Bohle, F. & Grimme, S. Automated exploration of the low-energy chemical space with fast quantum chemical methods. *Phys. Chem. Chem. Phys.* **22**, 7169-7192 (2020).

151 Del Galdo, S., Fusè, M. & Barone, V. The ONIOM/PMM Model for Effective Yet Accurate Simulation of Optical and Chiroptical Spectra in Solution: Camphorquinone in Methanol as a Case Study. *J. Chem. Theoy Comput.* **16**, 3294-3306 (2020).

152 Panek, P. T. & Jacob, C. R. Anharmonic Theoretical Vibrational Spectroscopy of Polypeptides. *J. Phys. Chem. Lett.* **7**, 3084-3090 (2016).

153 Roy, T. K., Sharma, R. & Gerber, R. B. First-principles anharmonic quantum calculations for peptide spectroscopy: VSCF calculations and comparison with experiments. *Phys. Chem. Chem. Phys.* **18**, 1607-1614 (2016).

154 Barone, V., Improta, R. & Rega, N. Quantum Mechanical Computations and Spectroscopy: From Small Rigid Molecules in the Gas Phase to Large Flexible Molecules in Solution. *Acc. Chem. Res.* **41**, 605-616 (2008).

155 Balabin, R. M. Conformational equilibrium in glycine: Focal-point analysis and ab initio limit. *Chem. Phys. Lett.* **479**, 195-200 (2009).

156 Bazsó, G., Magyarfalvi, G. & Tarczay, G. Tunneling Lifetime of the ttc/VIp Conformer of Glycine in Low-Temperature Matrices. *J. Phys. Chem. A* **116**, 10539-10547 (2012).

157 Stepanian, S. G. *et al.* Matrix-Isolation Infrared and Theoretical Studies of the Glycine Conformers. *J. Phys. Chem. A* **102**, 1041-1054 (1998).

158 Balabin, R. M. Conformational Equilibrium in Glycine: Experimental Jet-Cooled Raman Spectrum. *J. Phys. Chem. Lett.* **1**, 20-23 (2010).

159 Lockyear, J. F. *et al.* Isomer Specific Product Detection in the Reaction of CH with Acrolein. *J. Phys. Chem. A* **117**, 11013-11026 (2013).

160 Barone, V., Biczysko, M., Borkowska-Panek, M. & Bloino, J. A Multifrequency Virtual Spectrometer for Complex Bio-Organic Systems: Vibronic and Environmental Effects on the UV/Vis Spectrum of Chlorophyll-a. *ChemPhysChem* **15**, 3355-3364 (2014).

161 Gouterman, M. Spectra of porphyrins. *J. Mol. Spectrosc.* **6**, 138-163 (1961).

162 Rätsep, M. *et al.* Absorption-emission symmetry breaking and the different origins of vibrational structures of the ^1Q_y and ^1Q_x electronic transitions of pheophytin a. *J. Chem. Phys.* **151**, 165102 (2019).

163 Dixon, J. M., Taniguchi, M. & Lindsey, J. S. PhotochemCAD 2: a refined program with accompanying spectral databases for photochemical calculations. *Photochem. Photobiol.* **81**, 212-213 (2005).

164 Huang, X., Braams, B. J. & Bowman, J. M. Ab initio potential energy and dipole moment surfaces for $H_5O_2^+$. *J. Chem. Phys.* **122**, 044308 (2005).

165 Petit, A. S., Ford, J. E. & McCoy, A. B. Simultaneous Evaluation of Multiple Rotationally Excited States of H_3+, H_3O^+, and CH_5^+ Using Diffusion Monte Carlo. *J. Phys. Chem. A* **118**, 7206-7220 (2014).

166 Petit, A. S. & McCoy, A. B. Diffusion Monte Carlo Approaches for Evaluating Rotationally Excited States of Symmetric Top Molecules: Application to H_3O^+ and D_3O^+. *J. Phys. Chem. A* **113**, 12706-12714 (2009).

167 Sandler, P., Buch, V. & Clary, D. C. Calculation of expectation values of molecular systems using diffusion Monte Carlo in conjunction with the finite field method. *J. Chem. Phys.* **101**, 6353-6355 (1994).

168 Paesani, F. & Whaley, K. B. Rotational excitations of N_2O in small helium clusters and the role of Bose permutation symmetry. *J. Chem. Phys.* **121**, 5293-5311, doi:10.1063/1.1782175 (2004).

169 Cho, H. M. & Singer, S. J. Correlation Function Quantum Monte Carlo Study of the Excited Vibrational States of $H_5O_2^+$ *J. Phys. Chem. A* **108**, 8691-8702 (2004).

170 McCoy, A. B., Diken, E. G. & Johnson, M. A. Generating Spectra from Ground-State Wave Functions: Unraveling Anharmonic Effects in the $OH^-{\cdot}H_2O$ Vibrational Predissociation Spectrum. *J. Phys. Chem. A* **113**, 7346-7352 (2009).

171 Polavarapu, P. L. *et al.* A Single Chiroptical Spectroscopic Method May Not Be Able To Establish the Absolute Configurations of Diastereomers: Dimethylesters of Hibiscus and Garcinia Acids. *J. Phys. Chem. A* **115**, 5665-5673 (2011).

172 Debie, E. *et al.* A confidence level algorithm for the determination of absolute configuration using vibrational circular dichroism or Raman optical activity. *ChemPhysChem* **12**, 1542-1549 (2011).

173 Fusè, M. *et al.* Unbiased Determination of Absolute Configurations by vis-à-vis Comparison of Experimental and Simulated Spectra: The Challenging Case of Diplopyrone. *J. Phys. Chem. B* **123**, 9230-9237 (2019).

174 Bogaerts, J. *et al.* A combined Raman optical activity and vibrational circular dichroism study on artemisinin-type products. *Phys. Chem. Chem. Phys.* **22**, 18014-18024 (2020).

175 Johnson, J. L. *et al.* Dissymmetry Factor Spectral Analysis Can Provide Useful Diastereomer Discrimination: Chiral Molecular Structure of an Analogue of (−)-Crispine A. *ACS Omega* **4**, 6154-6164 (2019).

176 Hopmann, K. H. *et al.* Determining the Absolute Configuration of Two Marine Compounds Using Vibrational Chiroptical Spectroscopy. *J. Org. Chem* **77**, 858-869 (2012).

177 Covington, C. L. & Polavarapu, P. L. Similarity in Dissymmetry Factor Spectra: A Quantitative Measure of Comparison between Experimental and Predicted Vibrational Circular Dichroism. *J. Phys. Chem. A* **117**, 3377-3386 (2013).

178 Nicu, V. P. & Baerends, E. J. Robust normal modes in vibrational circular dichroism spectra. *Phys. Chem. Chem. Phys.* **11**, 6107-6118 (2009).

179 Tommasini, M. *et al.* Mode Robustness in Raman Optical Activity. *J. Chem. Theoy Comput.* **10**, 5520-5527 (2014).

180 Freedman, T. B., Shih, M.-L., Lee, E. & Nafie, L. A. Electron Transition Current Density in Molecules. 3. Ab Initio Calculations for Vibrational Transitions in Ethylene and Formaldehyde. *J. Am. Chem. Soc.* **119**, 10620-10626 (1997).

181 Fusè, M., Egidi, F. & Bloino, J. Vibrational circular dichroism under the quantum magnifying glass: from the electronic flow to the spectroscopic observable. *Phys. Chem. Chem. Phys.* **21**, 4224-4239 (2019).

182 Hug, W. Visualizing Raman and Raman optical activity generation in polyatomic molecules. *Chem. Phys.* **264**, 53-69 (2001).

183 Yamamoto, S. in *Introduction to Astrochemistry: Chemical Evolution from Interstellar Clouds to Star and Planet Formation* (Springer, Japan, 2017).

184 Jørgensen, J. K., Belloche, A. & Garrod, R. T. Astrochemistry During the Formation of Stars. *Annu. Rev. Astron. Astrophys.* **58**, 727-778 (2020).

185 McGuire, B. A. 2018 Census of Interstellar, Circumstellar, Extragalactic, Protoplanetary Disk, and Exoplanetary Molecules. *Astrophys. J., Suppl. Ser.* **239**, 17 (2018).

186 Herbst, E. & Dishoeck, E. F. v. Complex Organic Interstellar Molecules. *Annu. Rev. Astron. Astrophys.* **47**, 427-480 (2009).

187 Lattelais, M., Pauzat, F., Ellinger, Y. & Ceccarelli, C. Interstellar complex organic molecules and the minimum energy principle. *Astrophys. J.* **696**, L133-L136 (2009).

188 Puzzarini, C. & Barone, V. A never-ending story in the sky: The secrets of chemical evolution. *Phys. Life Rev.* **32**, 59-94 (2020).

189 Cernicharo, J., Guélin, M., Agúndez, M., McCarthy, M. C. & Thaddeus, P. Detection of C_5N^- and Vibrationally Excited C_6H in IRC+10216. *Astrophys. J.* **688**, L83-L86 (2008).

190 Botschwina, P. & Oswald, R. Carbon chains of type $C_{2n+1}N^-$ (n=2–6): A theoretical study of potential interstellar anions. *J. Chem. Phys.* **129**, 044305 (2008).

191 Cazzoli, G., Cludi, L., Buffa, G. & Puzzarini, C. Precise THz measurements of HCO^+, N_2H^+ and CF^+ for astrophysical observations. *Astrophys. J., Suppl. Ser.* **203**, 11 (2012).

192 Guzmán, V. *et al.* The hyperfine structure in the rotational spectrum of CF^+. *Astron. Astrophys.* **548**, A94 (2012).

193 Caselli, P., Myers, P. C. & Thaddeus, P. Radio-astronomical Spectroscopy of the Hyperfine Structure of N_2H^+. *Astrophys. J.* **455** (1995).

194 Kłos, J. & Lique, F. in *Cold Chemistry: Molecular Scattering and Reactivity Near Absolute Zero* (eds Dulieu O & Osterwalder A) Ch. Cold Molecular Collisions: Quantum Scattering Calculations and Their Relevance in Astrophysical Applications, 46-91 (RSC Publication, United Kingdom, 2018).

195 Borrego-Varillas, R. *et al.* Two-dimensional UV spectroscopy: a new insight into the structure and dynamics of biomolecules. *Chem. Sci.* **10**, 9907-9921 (2019).

196 East, K. W. *et al.* NMR and computational methods for molecular resolution of allosteric pathways in enzyme complexes. *Biophys. Rev.* **12**, 155-174 (2020).

197 Huang, J., Zhou, Y. & Xie, D. Predicted infrared spectra in the HF stretching band of the H_2–HF complex. *J. Chem. Phys.* **149**, 094307 (2018).

198 Clary, D. C. & Nesbitt, D. J. Calculation of vibration–rotation spectra for rare gas–HCl complexes. *J. Chem. Phys.* **90**, 7000-7013 (1989).

199 Felker, P. M. & Bačić, Z. H_2O–CO and D_2O–CO complexes: Intra- and intermolecular rovibrational states from full-dimensional and fully coupled quantum calculations. *J. Chem. Phys.* **153**, 074107 (2020).

200 Keutsch, F. N. & Saykally, R. J. Water clusters: Untangling the mysteries of the liquid, one molecule at a time. *Proc. Natl. Acad. Sci. U.S.A.* **98**, 10533-10540 (2001).

201 Mukhopadhyay, A., Xantheas, S. S. & Saykally, R. J. The water dimer II: Theoretical investigations. *Chem. Phys. Lett.* **700**, 163-175 (2018).

202 Schwan, R. *et al.* Observation of the Low-Frequency Spectrum of the Water Dimer as a Sensitive Test of the Water Dimer Potential and Dipole Moment Surfaces. *Angew. Chem. Int. Ed.* **58**, 13119-13126 (2019).

203 Cisneros, G. A. *et al.* Modeling Molecular Interactions in Water: From Pairwise to Many-Body Potential Energy Functions. *Chem. Rev.* **116**, 7501-7528 (2016).

204 Mallory, J. D. & Mandelshtam, V. A. Diffusion Monte Carlo studies of MB-pol $(H_2O)_{2-6}$ and $(D_2O)_{2-6}$ clusters: Structures and binding energies. *J. Chem. Phys.* **145**, 064308 (2016).

205 Liu, K. *et al.* Characterization of a cage form of the water hexamer. *Nature* **381**, 501-503 (1996).
206 Lee, V. G. M., Vetterli, N. J., Boyer, M. A. & McCoy, A. B. Diffusion Monte Carlo Studies on the Detection of Structural Changes in the Water Hexamer upon Isotopic Substitution. *J. Phys. Chem. A* **124**, 6903-6912 (2020).
207 Richardson, J. O. *et al.* Concerted hydrogen-bond breaking by quantum tunneling in the water hexamer prism. *Science* **351**, 1310-1313 (2016).
208 Vaillant, C. L., Wales, D. J. & Althorpe, S. C. Tunneling Splittings in Water Clusters from Path Integral Molecular Dynamics. *J. Phys. Chem. Lett.* **10**, 7300-7304 (2019).
209 Gaigeot, M. P. Unravelling the Conformational Dynamics of the Aqueous Alanine Dipeptide with First-Principle Molecular Dynamics. *J. Phys. Chem. B* **113**, 10059-10062 (2009).
210 Clary, D. C., Benoit, D. M. & van Mourik, T. H-Densities: A New Concept for Hydrated Molecules. *Acc. Chem. Res.* **33**, 441-447 (2000).
211 Fornaro, T., Burini, D., Biczysko, M. & Barone, V. Hydrogen-Bonding Effects on Infrared Spectra from Anharmonic Computations: Uracil–Water Complexes and Uracil Dimers. *J. Phys. Chem. A* **119**, 4224-4236 (2015).
212 Beć, K. B., Grabska, J., Ozaki, Y., Czarnecki, M. A. & Huck, C. W. Simulated NIR spectra as sensitive markers of the structure and interactions in nucleobases. *Sci. Rep.* **9**, 17398 (2019).
213 Beć, K. B. & Huck, C. W. Breakthrough Potential in Near-Infrared Spectroscopy: Spectra Simulation. A Review of Recent Developments. *Front. Chem.* **7** (2019).
214 Benoit, D. M. Rationalising the vibrational spectra of biomolecules using atomistic simulations. *Front. Biosci.* **14**, 4229-4241 (2009).
215 Atanasov, M., Ganyushin, D., Sivalingam, K. & Neese, F. in *Molecular Electronic Structures of Transition Metal Complexes II* (eds Mingos D M P, Day P, & Dahl J P) Ch. A Modern First-Principles View on Ligand Field Theory Through the Eyes of Correlated Multireference Wavefunctions, 149-220 (Springer, Berlin Heidelberg, 2012).
216 Singh, S. K., Atanasov, M. & Neese, F. Challenges in Multireference Perturbation Theory for the Calculations of the g-Tensor of First-Row Transition-Metal Complexes. *J. Chem. Theoy Comput.* **14**, 4662-4677 (2018).
217 Maganas, D. *et al.* First principles calculations of the structure and V L-edge X-ray absorption spectra of V_2O_5 using local pair natural orbital coupled cluster theory and spin–orbit coupled configuration interaction approaches. *Phys. Chem. Chem. Phys.* **15**, 7260-7276 (2013).
218 Roemelt, M., Maganas, D., DeBeer, S. & Neese, F. A combined DFT and restricted open-shell configuration interaction method including spin-orbit coupling: Application to transition metal L-edge X-ray absorption spectroscopy. *J. Chem. Phys.* **138**, 204101 (2013).
219 Neese, F. A critical evaluation of DFT, including time-dependent DFT, applied to bioinorganic chemistry. *J. Biol. Inorg. Chem.* **11**, 702-711 (2006).
220 Neese, F. High-Level Spectroscopy, Quantum Chemistry, and Catalysis: Not just a Passing Fad. *Angew. Chem. Int. Ed.* **56**, 11003-11010 (2017).
221 Neese, F., Atanasov, M., Bistoni, G., Maganas, D. & Ye, S. Chemistry and Quantum Mechanics in 2019: Give Us Insight and Numbers. *J. Am. Chem. Soc.* **141**, 2814-2824 (2019).
222 Zadrozny, J. M. & Long, J. R. Slow Magnetic Relaxation at Zero Field in the Tetrahedral Complex $[Co(SPh)_4]^{2-}$. *J. Am. Chem. Soc.* **133**, 20732-20734 (2011).
223 Neese, F. & Pantazis, D. A. What is not required to make a single molecule magnet. *Faraday Discuss.* **148**, 229-238 (2011).
224 Suturina, E. A. *et al.* Magneto-Structural Correlations in Pseudotetrahedral Forms of the $[Co(SPh)_4]^{2-}$ Complex Probed by Magnetometry, MCD Spectroscopy, Advanced EPR Techniques, and ab Initio Electronic Structure Calculations. *Inorg. Chem.* **56**, 3102-3118 (2017).

225 Suturina, E. A., Maganas, D., Bill, E., Atanasov, M. & Neese, F. Magneto-Structural Correlations in a Series of Pseudotetrahedral $[Co^{II}(XR)_4]^{2-}$ Single Molecule Magnets: An ab Initio Ligand Field Study. *Inorg. Chem.* **54**, 9948-9961 (2015).
226 Rechkemmer, Y. *et al.* A four-coordinate Cobalt(II) single-ion magnet with coercivity and a very high energy barrier. *Nat. Commun.* **7**, 10467 (2016).
227 Penocchio, E., Piccardo, M. & Barone, V. Semiexperimental Equilibrium Structures for Building Blocks of Organic and Biological Molecules: The B2PLYP Route. *J. Chem. Theoy Comput.* **11**, 4689-4707 (2015).
228 Kodrycka, M. & Patkowski, K. Platinum, gold, and silver standards of intermolecular interaction energy calculations. *J. Chem. Phys.* **151**, 070901 (2019).
229 Alessandrini, S., Gauss, J. & Puzzarini, C. Accuracy of Rotational Parameters Predicted by High-Level Quantum-Chemical Calculations: Case Study of Sulfur-Containing Molecules of Astrochemical Interest. *J. Chem. Theory Comput.* **14**, 5360-5371 (2018).
230 Dral, P. O. Quantum Chemistry in the Age of Machine Learning. *J. Phys. Chem. Lett.* **11**, 2336-2347 (2020).
231 Liakos, D. G., Guo, Y. & Neese, F. Comprehensive Benchmark Results for the Domain Based Local Pair Natural Orbital Coupled Cluster Method (DLPNO-CCSD(T)) for Closed- and Open-Shell Systems. *J. Phys. Chem. A* **124**, 90-100 (2020).
232 Nagy, P. R. & Kállay, M. Approaching the Basis Set Limit of CCSD(T) Energies for Large Molecules with Local Natural Orbital Coupled-Cluster Methods. *J. Chem. Theoy Comput.* **15**, 5275-5298 (2019).
233 Sibert III, E. L. Modeling vibrational anharmonicity in infrared spectra of high frequency vibrations of polyatomic molecules. *J. Chem. Phys.* **150**, 090901 (2019).
234 Basdogan, Y. *et al.* Machine Learning-Guided Approach for Studying Solvation Environments. *J. Chem. Theoy Comput.* **16**, 633-642 (2020).
235 Hodecker, M., Biczysko, M., Dreuw, A. & Barone, V. Simulation of Vacuum UV Absorption and Electronic Circular Dichroism Spectra of Methyl Oxirane: The Role of Vibrational Effects. *J. Chem. Theoy Comput.* **12**, 2820-2833 (2016).
236 Puzzarini, C., Biczysko, M., Bloino, J. & Barone, V. Accurate spectroscopic characterization of oxirane: a valuable route to its identification in Titan's atmosphere and the assignment of unidentified infrared bands. *Astrophys. J.* **785**, 107 (2014).
237 Karton, A., Sylvetsky, N. & Martin, J. M. L. W4-17: A diverse and high-confidence dataset of atomization energies for benchmarking high-level electronic structure methods. *J. Comput. Chem.* **38**, 2063-2075 (2017).
238 Mayhall, N. J. & Raghavachari, K. Molecules-in-Molecules: An Extrapolated Fragment-Based Approach for Accurate Calculations on Large Molecules and Materials. *J. Chem. Theoy Comput.* **7**, 1336-1343 (2011).
239 Santra, G., Sylvetsky, N. & Martin, J. M. L. Minimally Empirical Double-Hybrid Functionals Trained against the GMTKN55 Database: revDSD-PBEP86-D4, revDOD-PBE-D4, and DOD-SCAN-D4. *J. Phys. Chem. A* **123**, 5129-5143 (2019).
240 Kussmann, J. & Ochsenfeld, C. Preselective Screening for Linear-Scaling Exact Exchange-Gradient Calculations for Graphics Processing Units and General Strong-Scaling Massively Parallel Calculations. *J. Chem. Theoy Comput.* **11**, 918-922 (2015).
241 Doser, B., Lambrecht, D. S. & Ochsenfeld, C. Tighter multipole-based integral estimates and parallel implementation of linear-scaling AO–MP2 theory. *Phys. Chem. Chem. Phys.* **10**, 3335-3344 (2008).
242 Ma, Q. & Werner, H.-J. Scalable Electron Correlation Methods. 7. Local Open-Shell Coupled-Cluster Methods Using Pair Natural Orbitals: PNO-RCCSD and PNO-UCCSD. *J. Chem. Theoy Comput.* **16**, 3135-3151 (2020).
243 Becca, F. & Sorella, S. in *Quantum Monte Carlo Approaches for Correlated Systems* (Cambridge University Press, Cambridge, 2017).

244 Puzzarini, C. & Barone, V. The challenging playground of astrochemistry: an integrated rotational spectroscopy – quantum chemistry strategy. *Phys. Chem. Chem. Phys.* **22**, 6507-6523 (2020).

245 Biczysko, M., Krupa, J. & Wierzejewska, M. Theoretical studies of atmospheric molecular complexes interacting with NIR to UV light. *Faraday Discuss.* **212**, 421-441 (2018).

246 Raucci, U. *et al.* Ab-initio molecular dynamics and hybrid explicit-implicit solvation model for aqueous and nonaqueous solvents: GFP chromophore in water and methanol solution as case study. *J. Comput. Chem.* (2020).

247 Zhang, W., Kong, X., Liu, S. & Zhao, Y. Multi-coefficients correlation methods. *WIREs Comput. Mol. Sci.* **10**, e1474 (2020).

248 Gagliardi, L. *et al.* Multiconfiguration Pair-Density Functional Theory: A New Way To Treat Strongly Correlated Systems. *Acc. Chem. Res.* **50**, 66-73 (2017).

249 Bannwarth, C. *et al.* Extended tight-binding quantum chemistry methods. *WIREs Comput. Mol. Sci.*, e01493 (2020).

250 Loos, P.-F., Scemama, A. & Jacquemin, D. The Quest for Highly Accurate Excitation Energies: A Computational Perspective. *J. Phys. Chem. Lett.* **11**, 2374-2383 (2020).

251 Casanova-Páez, M. & Goerigk, L. Assessing the Tamm–Dancoff approximation, singlet–singlet, and singlet–triplet excitations with the latest long-range corrected double-hybrid density functionals. *J. Chem. Phys.* **153**, 064106 (2020).

252 Mutter, S. T. *et al.* Conformational dynamics of carbohydrates: Raman optical activity of D-glucuronic acid and N-acetyl-D-glucosamine using a combined molecular dynamics and quantum chemical approach. *Phys. Chem. Chem. Phys.* **17**, 6016-6027 (2015).

253 Lee, V. G. M. & McCoy, A. B. An Efficient Approach for Studies of Water Clusters Using Diffusion Monte Carlo. *J. Phys. Chem. A* **123**, 8063-8070 (2019).

254 Zhao, L. *et al.* Real-Time Time-Dependent Nuclear−Electronic Orbital Approach: Dynamics beyond the Born–Oppenheimer Approximation. *J. Phys. Chem. Lett.* **11**, 4052-4058 (2020).

255 Petrenko, T. & Rauhut, G. A General Approach for Calculating Strongly Anharmonic Vibronic Spectra with a High Density of States: The $\tilde{X}^2B_1 \leftarrow \tilde{X}^1A_1$ Photoelectron Spectrum of Difluoromethane. *J. Chem. Theoy Comput.* **13**, 5515-5527 (2017).

256 Cerezo, J., Aranda, D., Avila Ferrer, F. J., Prampolini, G. & Santoro, F. Adiabatic-Molecular Dynamics Generalized Vertical Hessian Approach: A Mixed Quantum Classical Method To Compute Electronic Spectra of Flexible Molecules in the Condensed Phase. *J. Chem. Theoy Comput.* **16**, 1215-1231 (2020).

257 Jasper, A. W., Harding, L. B., Knight, C. & Georgievskii, Y. Anharmonic Rovibrational Partition Functions at High Temperatures: Tests of Reduced-Dimensional Models for Systems with up to Three Fluxional Modes. *J. Phys. Chem. A* **123**, 6210-6228 (2019).

258 Burd, T. A. H. & Clary, D. C. Analytic Route to Tunneling Splittings Using Semiclassical Perturbation Theory. *J. Chem. Theoy Comput.* **16**, 3486-3493 (2020).

259 O'Connor, M. B. *et al.* Interactive molecular dynamics in virtual reality from quantum chemistry to drug binding: An open-source multi-person framework. *J. Chem. Phys.* **150**, 220901 (2019).

260 McArdle, S., Endo, S., Aspuru-Guzik, A., Benjamin, S. C. & Yuan, X. Quantum computational chemistry. *Rev. Mod. Phys.* **92**, 015003 (2020).